8-24-2016 12:00 AM

Parametric Design, Modeling, and Optical Evaluation of Retroreflective Prismatic Structures

Sama Hussein
The University of Western Ontario

Supervisor
Dr. Remus Tutunea-Fatan
The University of Western Ontario Joint Supervisor
Dr. Evgueni Bordatchev
The University of Western Ontario

Graduate Program in Mechanical and Materials Engineering
A thesis submitted in partial fulfillment of the requirements for the degree in Master of Engineering Science

Abstract

Retroreflectors (RR) are defined as passive optical structures that redirect incident light to its originating source. Specific types of retroreflectors called inverted cubes (ICs) function through total internal reflection (TIR) and are used in various applications such as measurement tools, traffic signs and automotive rear and side lighting. This thesis aims to model, analyze, fabricate and study a novel type of IC retroreflectors called right triangular prism (RTP). A parametric approach is used to model existing IC geometries from a generic unit cube and is then implemented to model the novel RTP geometry. Those elements are then tested by optical simulation software in single element and areal forms and their performances are compared. Moreover, fabricated prototype arrays of RTPs were separately tested using a digital lux meter and a luminance imaging system. Both virtual and physical optical experimentation proved that the newly designed RTP structure is indeed functional and have the potential to be used in many applications.

Keywords

Micro-optics, Retroreflector, Right Triangular Prism, Inverted Cube Retroreflector, Automotive Lighting, Reflex Reflector, Diamond Cutting

Co-Authorship Statement

Chapter 1: Sama Hussein – wrote manuscript

Chapter 2: Sama Hussein – designed study, performed analysis, wrote manuscript

Benjamin Hamilton – reviewed fabrication manuscript

Evgueni Bordatchev – supervised work, wrote and reviewed manuscript

Remus Tutunea-Fatan – supervised work, reviewed manuscript

Chapter 3: Sama Hussein – designed study, performed analysis, wrote manuscript

Benjamin Hamilton – fabricated arrays, performed analysis, wrote manuscript

Evgueni Bordatchev – supervised work, reviewed manuscript

Remus Tutunea-Fatan – supervised work, reviewed manuscript

Chapter 4: Sama Hussein – designed study, performed analysis, wrote manuscript

Benjamin Hamilton –fabricated arrays

Remus Tutunea-Fatan – supervised work, reviewed manuscript

Evgueni Bordatchev – supervised work, reviewed manuscript

Chapter 5: Sama Hussein – wrote manuscript

Dedications

This thesis is dedicated to my loving parents as they have always inspired me to learn, and without whom none of this would be possible.

Acknowledgments

First and foremost, I would like to deeply thank my supervisors, Dr. Remus Tutunea-Fatan and Dr. Evgueni Bordatchev for the unconditional support and encouragement they have provided throughout my degree. Dr. Tutunea, words cannot express my appreciation for all the help, patience and overtime you granted me. You always made yourself available regardless of your schedule and I always knew you will be present to address any concerns. Dr. Bordatchev, thank you for your invaluable advice and support. You were always patient with me and always willing to put some time aside for the sake of research. Truly your guidance was beyond the scope of a normal supervisor.

I would also like to thank my research partners Ben Hamilton and Nicolas Milliken. Ben, you have always been a great example an ethical, trustworthy and supportive peer, and I have really enjoyed working along with you. Nic, your help with the experiments was priceless and it has really been a great privilege working with you. I wish you all the best with the rest of your work.

In addition, I would like to thank my colleagues Shirzad Mohajerani, Mohammadreza Faieghi, Navraj Heer, Mahdi Bagheripoor, and Josh Miller for being a part of this trip and for offering a hand when needed.

My masters would have been much more difficult without the continuous moral support and advice my friends Somiraa Said and Melissa Salem have given me. Somiraa, I am genuinely grateful for every moment you were there with me, and for your constant guidance. Melissa, your cheerful presence was always a great relief to all my worries and concerns.

I would like to express my sincere gratitude to my parents, Alaa Abuldhady and Doaa Lashin, as they have sacrificed so many things in their lives to invest in my education and have always been there for me with their never ending support.

I am sincerely grateful to the “Ontario Graduate Scholarship” and the “BMO Financial Group Ontario Graduate Scholarships” as I have had the privilege to hold this honorable award. Finally, this research was conducted in collaboration with Canada’s National Research Council (NRC) that provided me with the facilities needed to make this work possible.

Table of Contents

List of Tables

List of Figures

List of Appendices

List of Abbreviations

CAD	computer-aided design
CAM	computer-aided manufacturing
CC	corner cube
IC	inverted cube
ICC	inverted corner cube
HA	hexagonal aperture
LED	light emitting diode
OEM	original equipment manufacturer
PMMA	polymethyl methacrylate
RR	retroreflector
RRE	retroreflection efficiency
RTP	right triangular prism
SEM	scanning electron microscopy
TA	triangular aperture
TIR	total internal reflection
USPIC	ultraprecise single point inverted cutting

CHAPTER 1

Introduction

1.1 Micro-Optics

The technology of micro-optics was initiated 20-30 years ago and since then has been emerging in various fields ranging from medicine to entertainment. The term micro-optics can be distinguished from optics through different aspects. For instance, it can be seen as the field of studying and designing optics at a miniature level (i.e. sub mm and sub μm level). However, some argue that there is no explicit definition of micro-optics in terms of size, and therefore, should be defined based on its microfabrication techniques (Herzig, 2000; Sinzinger and Jahns, 2006; Zappe, 2010).

Although the expression of micro-optics only appeared in the 1980s (Iga *et al.*, 1984), some components have been around from before. The development of micro-optics was limited by the high-cost microfabrication processes. For instance, in 1874 Lord Rayleigh started using gratings for spectroscopy instead of prisms as they showed better resolution, but those gratings did not replace prisms in this application until the 1950s due to their expensive fabrication process. The costs of the manufacturing process later reduced with the developing replication technology which opened the door for mass producing high-precision gratings from a single expensive master piece (Zappe, 2010). This replication process later opened the opportunity to a wide range of applications and is still one of the main processes used in fabrication of micro-optics till the today.

Present-day field of micro-optics is associated with various technologies that continue to broaden its scope of applications (Borrelli, 2004; Sinzinger and Jahns, 2006; Kress and Meyrueis, 2009; Zappe, 2010). Fabrication techniques of micro-optics can be branched into two subdivisions: lithographic such as optical, electron beam, X-ray, and non-lithographic such as diamond cutting and microjet printing (Sinzinger and Jahns, 2006).

The arrival for the lithographic techniques provided new opportunities for fabrication of micrometer accuracy diffractive micro-optics and microlenses (Sinzinger and Jahns, 2006; Zappe, 2010). Non-lithographic techniques, on the other hand, such as diamond cutting are being recently inspected in an effort to further reduce fabrication costs and produce complex geometries (Sinzinger and Jahns, 2006). Moreover, extra precise processes such as diamond micro chiseling are being investigated to create further complex optical elements whose geometries are a limit to the available machining capabilities. This process can be very helpful in miniaturizing optical elements such as reflective or refractive elements, used for automotive lighting, and reflective foils for traffic signs or safety garments to a scale of a few microns (Herzig, 1997; Brinksmeier *et al.*, 2008; Brinksmeier *et al.*, 2012b; Hamilton *et al.*, 2016b).

1.2 Micro-Optical System Modeling

The science of micro-optics can be understood through designing practical systems that control passive (*e.g.* taillight retroreflectors) and active (*e.g.* automotive headlamps) optical elements to achieve the required results. Computer and modeling simulations are very useful tool as they save an optical engineer cost and time. Optical simulation systems work through ray tracing, in which a light ray is envisioned as a line normal to the direction of the electromagnetic wave propagation. As a light ray passes through different optical elements, the computer recalculates the direction of the rays by following the basic optical concepts such as transmission, reflection, refraction, etc. A ray tracing system can be divided into two major parts: sequential and non-sequential modeling. A sequential model is a system in which the rays pass through objects in order of their positions whereas, in a

non-sequential ray tracing, the rays do not necessarily hit the optical elements in the order they are placed in (Taylor, 2000).

1.3 Retroreflectors

Retroreflection is the optical phenomenon in which light is guided to a direction that is opposite and parallel to that of the originating source, and the passive optical structures that help achieve this aspect are called retroreflectors (RRs). RRs are commonly used in a wide scope of applications such as metrology, road safety and interferometers (Liepmann, 1994).

Retroreflectors operate using two simple optical concepts: reflection and refraction. Reflection is the redirection of light to an angle equal in magnitude and opposite in direction to the incidence angle, while refraction is the deviation of a light ray as it passes from one medium to another which can be expressed through Snell's law (Equation 1.1).

$$\frac{n_1}{n_2}=\frac{\sin\theta_1}{\sin\theta_2} \qquad [1.1]$$

Generally, when a light ray passes from a region of a high refractive index to one with lower refractive index, a portion of that light gets reflected and the rest are refracted away from the normal so that the angle of refraction is greater than the incidence angle. When the incidence angle reaches a certain critical angle, θ_c, the light exits at an angle of 90° to the normal. Moreover, if the light strikes the medium at any angle greater than that critical angle, it gets completely reflected and no refraction occurs. This phenomenon is called total internal reflection (TIR) (Taylor, 2000). This critical angle can be calculated from the

refractive indices of the two mediums through Equation 1.2, where n_1 and n_2 are the refractive indices of the first and second mediums, respectively.

$$\theta_c = \sin^{-1}\left(\frac{n_2}{n_1}\right) \qquad [1.2]$$

Figure 1.1 shows an example of a light ray passing from polymethyl methacrylate, PMMA, (n_{PMMA}=1.492) to air (n_{air}= 1) at different angles of incidence. The critical angle in this case is 42.11°. Therefore, if the light hits the air at an angle greater than 42.11°, TIR will take place and all the light will be reflected; if it strikes the air at angle equal to 42.11°, the refracted way will travel along the surface of PMMA, and if it hits at an angle lower than 42.11°, it will be refracted.

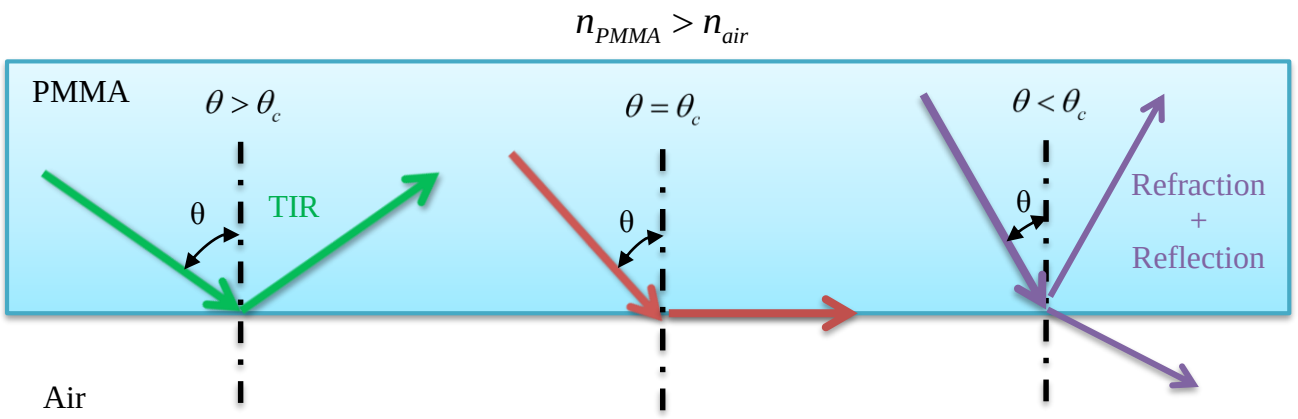

Figure 1.1: Total internal reflection

1.3.1 Types of Retroreflectors

There are different types of retroreflectors that essentially all serve the same purpose but work in different ways to do so. The three main types of retroreflective elements currently

used in commercial applications are lens and mirror, corner cube (CC) and inverted cube (IC) retroreflectors.

Lens and mirror, also known as cat's eye, RRs are commonly used as warning and traffic calming devices in local roads and highways such as in the retroreflective sheets used on stop signs (Medicus, 2006). As their name indicates they consist of a lens and a mirror which work together to achieve retroreflection as seen in Figure 1.2. This setup functions in a similar pattern to a cat's eye, which glows at night when light is directed towards it.

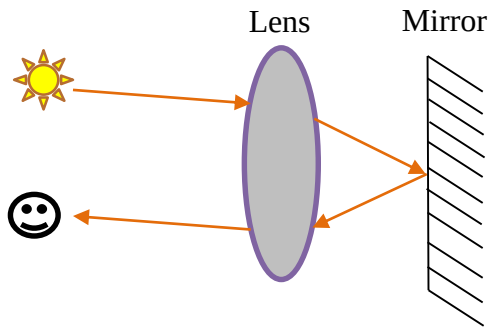

Figure 1.2: Lens and mirror retroreflector

On the other hand, corner cube (CC) RRs use two or three reflective surfaces to achieve retroreflection. This type of RR simply works by reflecting light rays from one reflective facet to another until they end up being oriented in a direction that is opposite and parallel to that of the originating source. Those reflective facets can be made of mirrors or highly polished metal surfaces.

If a corner cube (CC) element were to be used as a master mold, the product mold would be in the shape of an inverted cube (IC) as shown in Figure 1.3, *i.e.* ICs represent the opposite/reverse side of the CCs. Inverted cubes function in a very similar manner to CCs

but by reflecting light through TIR. They are usually made of transparent materials such as glass or plastic and they depend on the fact that the refractive indices of these materials are higher than that of air. Figure 1.3 shows images of CC and IC RRs retroreflecting light.

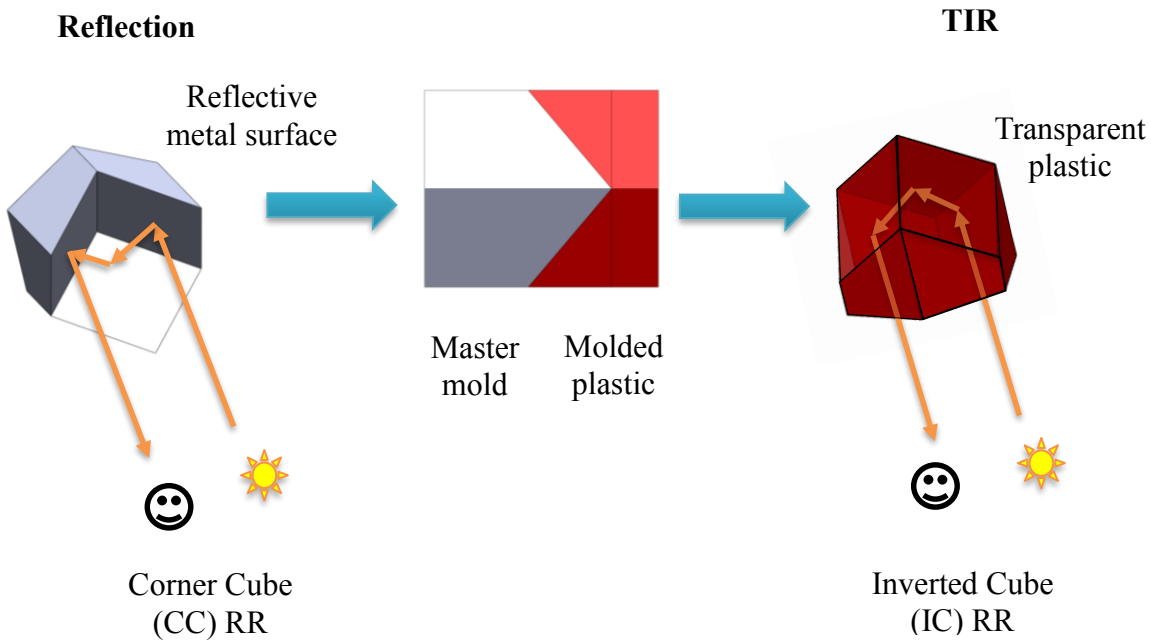

Figure 1.3: Working principle of CC and IC RRs

1.3.2 Optical Evaluation Metrics of ICs

There are five main metrics used to evaluate the optical performance of an RR: retroreflection efficiency, divergence, angularity, brilliancy. and effective retroreflective area. Retroreflection efficiency (RRE) is the ratio of retroreflected light to the incident light. Divergence evaluates the amount of deviation of the retroreflected light from the incidence light, whereas, angularity corresponds to range of incidence angles at which the RR is able to function and is greatly limited by the critical angle needed for TIR to occur in an IC RR. Brilliancy is the retroreflection efficiency at specified observation angles (Lundvall *et al.*, 2003). The aforementioned four optical evaluation metrics can be used to

evaluate any RR. Effective retroreflective area, on the other hand, can only be related to CC or IC RRs and it correlates to the percentage of incident facet area participating in retroreflection (Kim and Lee, 2007).

Some of those performance specifications are inversely related to each other. Therefore, it is important to fabricate the RRs to fit the required criteria according to various applications. For instance, RRE and divergence angles are the most essential prerequisites of an RR used in safety applications (Yuan *et al.*, 2002). Therefore, RRs used in automotive tail and side lightings are required to follow specific safety standards that dictate certain amount of RRE at given divergence angles.

1.3.3 Applications of Retroreflectors

Lens and mirror RRs are typically used for safety applications as they have a wide angularity, whereas, CC and ICC RRs are preferred in measurement applications as they require higher RRE (Seward and Cort, 1999; Brinksmeier et al., 2012a). However, all three RRs are often interchanged in many fields of applications due to specific requirements (*e.g.* RRE) or limitations (*e.g.* cost).

For instance, CC RRs have been used for Lunar Laser Ranging after the Apollo mission planted 11 retroreflective arrays on the moon in 1969 (Erickson, 2011). Since then, they have produced comprehensive information about the crust and interior of the moon and have resulted in some of the best tests in the field of general relativity (Currie et al., 2011).

Moreover, RRs have been used in the traffic world for many years. In 1920s RRs were first introduced to traffic signs by attaching relatively large glass spheres (10 mm - 20 mm) or glass moldings of prismatic elements (6 mm) to them (Lloyd, 2008). Present-day traffic

signs, however, have their history in the miniaturization of these two retroreflective elements. In the 1930s, glass spheres, which act as lens and mirror RRs, of a diameter less than 1 mm were first used in the cinemas to produce much brighter images. Those glass spheres later went through a development process by 3M in an effort of integrating them in traffic signs and road pavements. The first glass beads embedded sheeting was implanted on outskirts in 1939 which later developed into a commercial sheeting product. Those sheets, however, only retroreflected at most 8% of the light. In 1971, 3M launched its new high intensity sheeting that has an RRE of 16% after applying refinements to both the retroreflective elements and the adhesive layer in which the glass spheres were enclosed. This sheeting was intensively used in major traffic signs mostly on high speed roads where night time visibility is a safety issue and is still used until today (Lloyd, 2008).

On the other hand, micro-prismatic sheeting, which acts as an array of IC RRs, was patented by the American Rowland brothers in 1970 and was first commercialized in 1973. In the 1989 3M launched its so-called “Diamond Grade” micro-prismatic sheeting which retroreflected 35% of incident light and proved to be more efficient than the glass beads sheets. Moreover, those micro-prismatic sheets provided refinement to car headlight designs and allowed them to focus more light onto the road surface which in turn was able to reduce the light on the roads. Those IC RR elements were and still are best suited to conditions where long range visibility is essential and where the direction of the oncoming traffic is head on (Lloyd, 2008). However, prismatic structures had some limitations as they were more expensive to fabricate, and less effective when viewed from wide angles (So *et al.*, 2002; Lundvall *et al.*), and therefore the glass bead sheets are still commonly used for general purpose traffic signs.

Nowadays the performance of retroreflective prismatic sheeting can be tailored to required applications through computer-aided design (CAD) and computer-aided manufacturing (CAM) technologies and are still continuously developing while trying to cut down their costs. Hence, it seems that although both micro-prismatic and glass beads retroreflective elements continue to coexists, the future potential mainly lies in the newly developing prismatic elements (Lloyd, 2008).

Furthermore, IC RR arrays, better known as reflex reflectors, are integrated in the automotive vehicles' rear and side lighting lamps to provide safety and visibility of the preceding traffic and safety standards are used to guide the performance of those RRs (Wördenweber *et al.*, 2007; SAE, 2009). For instance, SAE standards require vehicles to have a minimum of two red RR arrays on the rear of the vehicle on each side of the centerline, and two arrays on each side of the vehicle, the front being amber in color and the back one being in red (Wördenweber *et al.*, 2007). This standard also provides other information guiding the position, reflectivity, area and visibility of the RR arrays integrated in rear and side lighting (SAE, 2009).

1.3.4 Inverted Cube Retroreflectors

Previous studies indicate that inverted cube retroreflectors acquire higher retroreflection efficiency than both corner cube and lens and mirror retroreflectors as the reflectivity acquired through TIR is higher than that acquired by normal reflection (Yuan *et al.*, 2002; Lloyd, 2008). Figure 1.4 shows the approach through which the reflective facets of a typical IC RR work together to achieve retroreflection. The light first enters through the incident facet and hits the first reflective facet which reflects light onto the second reflective facet

through TIR, and then to the third and finally leaves the RR element in a direction to that of the incident one.

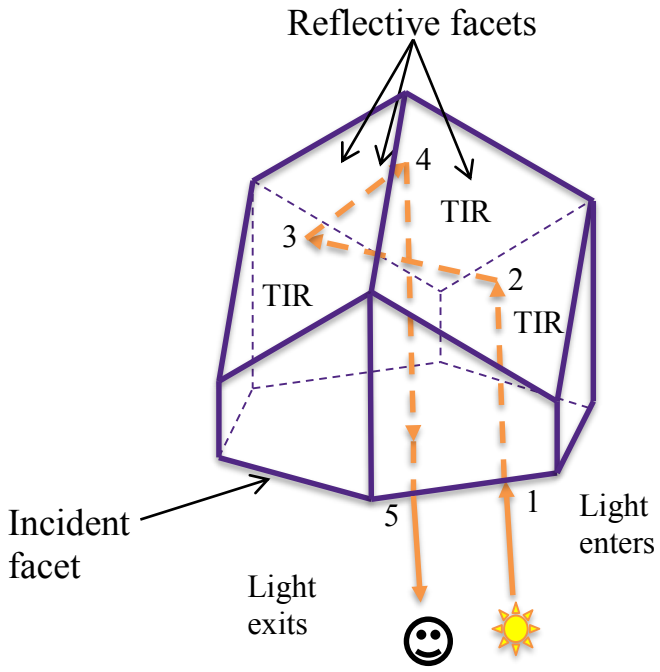

Figure 1.4: Inverted cube retroreflector

Present day commercial applications use a specific type of ICs called inverted corner cube (ICC) which consists of three reflective orthogonal facets. ICCs have been used for decades in safety applications in the form of triangular and hexagonal aperture elements. This thesis however focuses on introducing, modeling, fabricating and testing a novel type of IC elements that consists of two reflective facets called right triangular prism (RTP). In addition, all types of ICs outlined in Figure 1.5 will be further modeled and elaborated on.

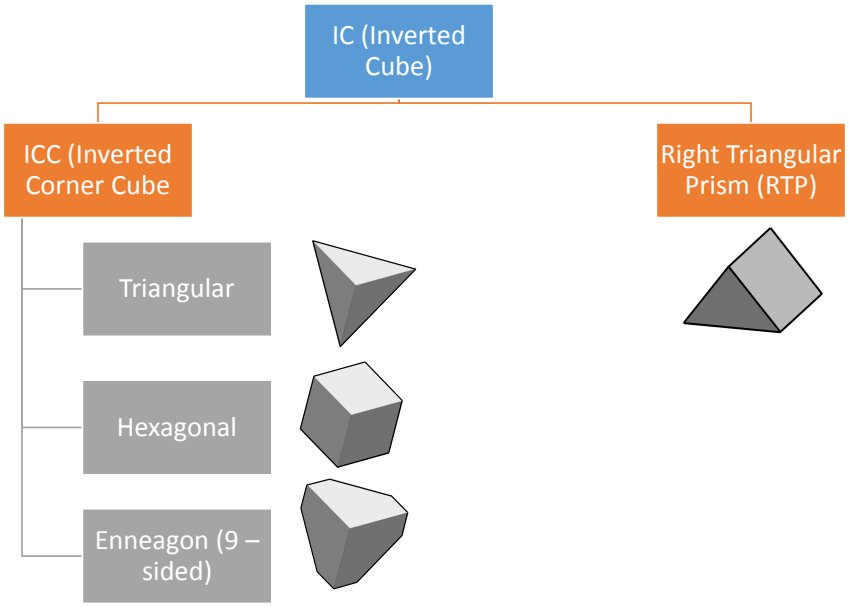

Figure 1.5: Types of inverted cube (IC) retroreflectors

1.4 Rationale

1.4.1 Motivation

The master mold used to produce IC RR arrays is usually fabricated by means of a method called pin bundling technique (Van Arnam, 1981; Brinksmeier *et al.*, 2008). Molds produced through this technique could take up to about 14 weeks and could cost around \$2000/in^2-\$3000/in^2, which implies that this fabrication method is both expensive and time consuming. Furthermore, this fabrication approach represents a limiting factor for both geometrical complexity and dimensional size of the retroreflectors that can only be of inverted cube type and of approximately 1-2 mm depth. Both constraints are determined by the geometry of the forming tip of the pin, as well as the way in which the pins are bundled/assembled together prior to electroforming. In theory, pins with smaller cross sectional sizes could also be used, but this will significantly increase their own

fabrication/handling costs and in turn, this will lead to higher overall mold production expenditures.

Pin-bundling technology represents the state-of-the-art technology used in the fabrication of the retroreflective components based on total internal reflection principles whose primary market continue to remain automotive lighting. However, it is important to point out that this technology has significantly restricted the geometrical diversity of this type of retroreflectors to the point that they have only been produced in ICC shape.

As a consequence of the severe manufacturing limitations, the current ICC design was used for decades without knowing much if it can be improved in any way in a sense that little – if anything – was published on the functionality of IC RRs or on how their design should be changed to improve their optical efficiency. This contradicts on many levels the classical product development paradigm shown in Figure 1.6 according to which extensive design, optimization and analysis should always precede the mass production phase.

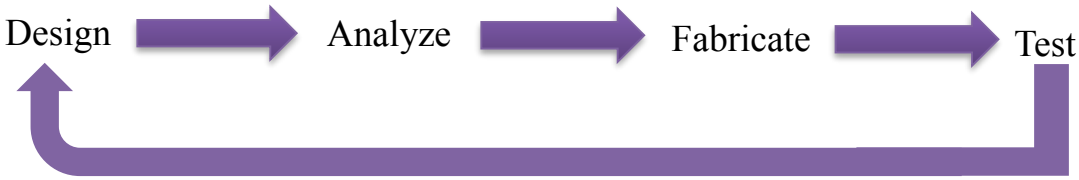

Figure 1.6: Product development process

To address the aforementioned manufacturing limitation of the traditional pin-bundling technique, ultraprecise single point inverted technique (USPIC) was developed by Hamilton et al. (Hamilton *et al.*, 2016a) The introduction of this new versatile fabrication technique unlocked a practically unlimited diversity of TIR-based RR geometries, and it

becomes clear that a need to develop a novel framework capable of modeling, designing, analyzing and ranking virtually any type of retroreflective geometry exists.

1.4.2 Contributions

The present thesis represents one of the first attempts to propose an integrated framework for the optical analysis of the TIR-based RRs. Hence, the major contributions of this thesis are related to the parametric approach proposed, developed and implemented for the modeling, designing and virtual/physical testing of new retroreflective elements called right triangular prisms (RTPs). While these retroreflective elements might be regarded as somewhat of a "case study" geometry in the context of the developed framework, the analysis reported in this thesis suggests that RTPs have equivalent – if not even better – optical performance when compared to their traditional ICC counterparts.

1.4.3 Objective

The main objectives of this thesis are:

1. to develop a parametric approach for designing and modeling inverted corner cube retroreflectors (ICC RRs) from a unit cube,

2. to develop a parametric model of a novel type of retroreflective elements termed as right triangular prism (RTP),

3. to study the optical performance of the designed and fabricated RTPs, and

4. to evaluate and compare the optical performance of the RTPs with respect to conventional ICC retroreflective structures.

1.4.4 Thesis Overview

Chapter 2 introduces the types of IC RRs and their functionalities in the scope of automotive tail and side lighting. Optical simulation testing is used to examine the effect of changing the orientation of the reflective facets in an IC RR as they deviate from the perpendicularity position. Moreover, it details the conventional pin bundling fabrication technique used to make the automotive rear and side lighting master molds, and examines the effects of manufacturing defects on the optical performance of IC RRs specifically in terms of retroreflection efficiency (RRE). Finally, parametric design and modeling is introduced on three different levels for future evaluation and optimization of optical performance of IC retroreflective elements according to the automotive tail and side lighting industry.

Chapter 3 introduces and details the parametric approach used to model the currently used ICC geometries from a unit cube through performing rotation and transformation operations. This approach is then adapted and implemented to model the novel right triangular prim (RTP) IC geometry using the same unit cube as a source and the same logic but with different operations. The chapter then specifically examines the effect of the presence of an illumination element on the RTP RR through a set of optical simulations. Moreover, the fabrication of the IC RRs through both conventional pin bundling and novel ultraprecise single point inverted cutting methods are discussed and the final geometries of both outputs are compared. Finally, the functionality of a fabricated RTP prototype array is tested through a real life setup.

Chapter 4 aims to use the parametric approach developed earlier in Chapter 3 to model three different IC elements and perform a comparative analysis between the their

retroreflection efficiencies (RREs) and effective retroreflective areas. The analysis is done via optical simulation software, OpticStudio, in which incidence angles were changed and results were measured. Experimental luminance measuring tests were then conducted using an RTP prototype, fabricated through ultraprecise single point inverted cutting (USPIC), and a conventional HA ICC array to prove the functionality of the novel RTP elements and their future potential to be commercialized in certain applications.

Chapter 5 sets a conclusion to the thesis and provides future recommendations.

1.5 References

Borrelli, N. F. 2004. *Microoptics Technology: Fabrication and Applications of Lens Arrays and Devices*, CRC Press.

Brinksmeier, E., Gläbe, R. & Flucke, C. 2008. Manufacturing of molds for replication of micro cube corner retroreflectors. *Production Engineering*, **2**, 33-38.

Brinksmeier, E., Glabe, R. & Schonemann, L. 2012a. Diamond Micro Chiseling of large-scale retroreflective arrays. *Precision Engineering-Journal of the International Societies for Precision Engineering and Nanotechnology*, **36**, 650-657.

Brinksmeier, E., Gläbe, R. & Schönemann, L. 2012b. Review on diamond-machining processes for the generation of functional surface structures. *CIRP Journal of Manufacturing Science and Technology*, **5**, 1-7.

Currie, D., Dell'Agnello, S. & Delle Monache, G. 2011. A Lunar Laser Ranging Retroreflector Array for the 21st Century. *Acta Astronautica*, **68**, 667-680.

Erickson, K. 2011. *What Neil and Buzz Left on the Moon* [Online]. NASA. Available: http://science.nasa.gov/science-news/science-at-nasa/2004/21jul_llr/ [Accessed July 26 2016].

Hamilton, B. W., Hussein, S., Milliken, N., Tutunea-Fatan, O. R. & Bordatchev, E. V. 2016a. Fabrication of Right Triangular Prism Retroreflectors Through 3½½-Axis Ultraprecise Single Point Inverted Cutting. *Computer-Aided Design and Applications*.

Hamilton, B. W., Hussein, S., Tutunea-Fatan, O. R. & Bordatchev, E. V. Fabrication of Right Triangular Prism Retroreflectors Through Ultraprecise Single Point Inverted Cutting. Manufacturing Science and Engineering Conference, April 12-15, 2016 2016b Columbia, SC, USA. ASME.

Herzig, H. P. 1997. *Micro-Optics: Elements, Systems, and Applications,* London, Taylor & Francis.

Herzig, H. P. 2000. The world of micro-optics. *Leos 2000 - Ieee Annual Meeting Conference Proceedings, Vols. 1 & 2,* 639-640.

Iga, K., Kokobun, Y. & Oikawa, M. 1984. *Fundamentals of Microoptics,* New York, Academic Press.

Kim, H. & Lee, B. 2007. Optimal design of retroreflection corner-cube sheets by geometric optics analysis. *Optical Engineering,* **46**.

Kress, B. C. & Meyrueis, P. 2009. *Applied Digital Optics: From Micro-optics to Nanophotonics,* Wiley.

Liepmann, T. W. 1994. How Retroreflectors Bring the Light Back. *Laser Focus World,* **30**, 129-132.

Lloyd, J. 2008. A brief history of retroreflective sign face sheet materials. [Accessed July 24, 2016].

Lundvall, A., Nikolajeff, F. & Lindstrom, T. 2003. High performing micromachined retroreflector. *Optics Express,* **11**, 2459-2473.

Medicus, K. M. 2006. *Improving Measurements Based on the Cat's Eye Retro-reflection.* Doctor of Philosophy, The University of North Carolina at Charlotte.

SAE 2009. Reflex Reflectors. *Surface Vehicle Standard.* SAE.

Seward, G. H. & Cort, P. S. 1999. Measurement and characterization of angular reflectance for cube-corners and microspheres. *Optical Engineering,* **38**, 164-169.

Sinzinger, S. & Jahns, J. 2006. *Microoptics,* Wiley.

So, B. S., Jung, Y. H. & Lee, D. W. 2002. Shape design of efficient retroreflective articles. *Journal of Materials Processing Technology,* **130**, 632-640.

Taylor, A. E. F. 2000. *Illumination Fundamentals,* US, Rensselaer Polytechnic Institute.

Van Arnam, D. E. 1981. Method for forming retroreflective sheeting. Google Patents.

Wördenweber, B., Wallaschek, J., Boyce, P. & Hoffman, D. D. 2007. *Automotive Lighting and Human Vision,* Springer Berlin Heidelberg.

Yuan, J., Chang, S., Li, S. & Zhang, Y. 2002. Design and fabrication of micro-cube-corner array retro-reflectors. *Optics Communications,* **209**, 75-83.

Zappe, H. 2010. *Fundamentals of Micro-Optics,* Cambridge University Press.

CHAPTER 2

Parameter-Driven Retroreflective Features

A version of this chapter was published as: Hussein, S., Hamilton, B., Bordatchev, E.V., and Tutunea-Fatan, O.R., 2015. Parameter-Driven Geometric Modeling of Retroreflective Features. *USB Proceedings of the* 25th *Canadian Congress of Applied Mechanics* (*CANCAM 2015*), Jun. 2015, London, Canada, pp. 96-99.

2.1 Overview

Retroreflectors (RR) are passive optical components that reflect the incident light back to its original source. Because of this characteristic, RRs are used in a broad palette of applications ranging from metrology to traffic safety. Among the variety of possible geometries of RRs, there are three main types of inverted cube (IC) shapes with different apertures: right triangular prism, triangular aperture and hexagonal aperture. While all types of RRs are capable of fulfilling their primary retroreflection function, their optical performances tend to make them more or less suitable to a particular application. In this regard, the present study is primarily focused on the application of IC RRs for automotive taillights. Non-sequential optical modeling of RRs has been used to outline their basic optical functionalities and to analyze the trajectory of the retroreflected light caused by the total internal reflection (TIR) phenomenon. Based on this, a parametric approach to define the principal geometric parameters of IC RRs is proposed by considering three levels of design parametrization: internal, areal and directional. The present study opens up new optical methods to be used in optimization and control of the optical performance for IC RRs in terms of the retroreflection efficiency and vertical/horizontal divergence.

2.2 Introduction

Retroreflection is an optical phenomenon characterized by an intentional reflection of the incoming light back to its original source(s) with a controlled amount of scattering (Liepmann, 1994; Nilsen and Lu, 2004). This optical functionality is critically required in safety applications involved in automotive and surface transportation (e.g. roadside markers, lighting, safety jackets/signs, etc.). Generally speaking, three main types of RR geometries have been used so far in almost all automotive lighting applications: lens-and-

mirror (also called cat's eye), corner cube (CC) and inverted corner cube (IC). The basic functionality of these RRs is depicted in Figure 2.1.

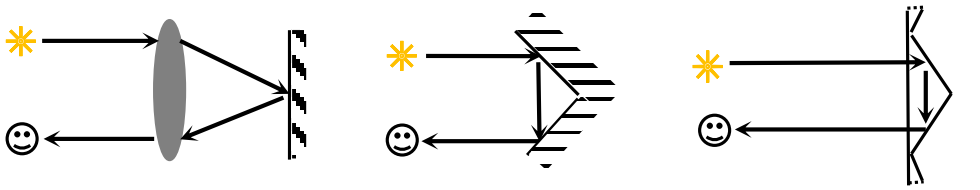

a) lens and mirror b) corner cube (CC) c) inverted cube (IC)

Figure 2.1: Principal retroreflector designs

In the lens-and-mirror (cat's eye) RR (see Figure 2.1a), the incoming light ray is directed towards a reflective surface and reflected back through a lens such that it is returned in a direction parallel to that of the incident ray. The CC RR typically consists of two or more mutually orthogonal reflective surfaces that are also capable to return the incident ray in a parallel direction (Figure 2.1b). However, no lens is required in this case since the return of the incident light is caused by the particularities of the RR geometry that speculates on the equivalence between incidence and reflection angles. CC RRs are known to have higher reflectivity than cat's eye designs although the latter ones can accept higher range of incident angles (So *et al.*, 2002). Finally, IC RRs (Figure 2.1c) are based on a different optical phenomenon called total internal reflection (TIR). Here, the incident ray is reflected at critical angle by an interface between two optical mediums with different indexes of refraction. This type of RRs is widely utilized in automotive lighting and it will constitute the main focus of the present study as it is believed to have the best future potential amongst other types of retroreflectors due to their superior retroreflection efficiency (Lloyd, 2008).

2.3 Working Principles, Fabrication and Typical Designs

In general terms, the IC RRs used in automotive rear and/or side lighting applications have to adequately and concurrently serve both safety and illumination functions (Figure 2.2). For this purpose, the typical design of an IC RR is comprised of an array of elementary features like the one shown in Figure 2.1c. This design ensures that the light reflected by the tailgate RR of the preceding car is returned to the succeeding vehicle, such that its driver is made aware of a preceding traffic hazard. On the other hand, the retroreflective element incorporates multiple illumination/signaling/brake warning functionalities that allow the driver of the preceding car to communicate his/her presence and/or actions/intentions. It is important to point out that in addition to the aforementioned traffic-related functions, rearlights are also required to meet aesthetic/styling requirements derived from their placement on the visible exterior of the automobile. However, this type of design constraints is not specifically considered within the limited scope of this work.

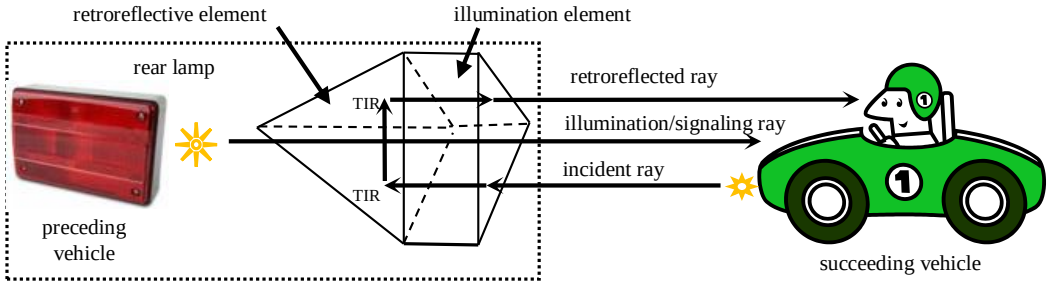

Figure 2.2: Optical functionality of the retroreflectors

To successfully meet their two principal functionalities, most taillights incorporate both illumination and retroreflective elements. While the actual embodiment broadly varies among manufacturers, illumination is typically ensured by a cut-off piece/bezel forming

the exterior surface of the lamp. By contrast, retroreflectivity is provided by means of the RR that is attached to the illumination system.

Commonly, each of the elementary RRs embedded in a rear lighting system has one ceiling/top incidence facet and at least two retroreflective facets. As a consequence, the incident light penetrates the optical body of the RR through the top facet and is then reflected back at the interface formed between air and lamp material which constitutes the core of the TIR phenomenon. Because of this, the angle formed by the retroreflective surfaces represents one of the most critical elements of RR design. Figure 2.3 clearly demonstrates that relatively small deviations from the optimal 90° value will cause dramatic decreases in the ratio between the reflected and incident power of the light beam.

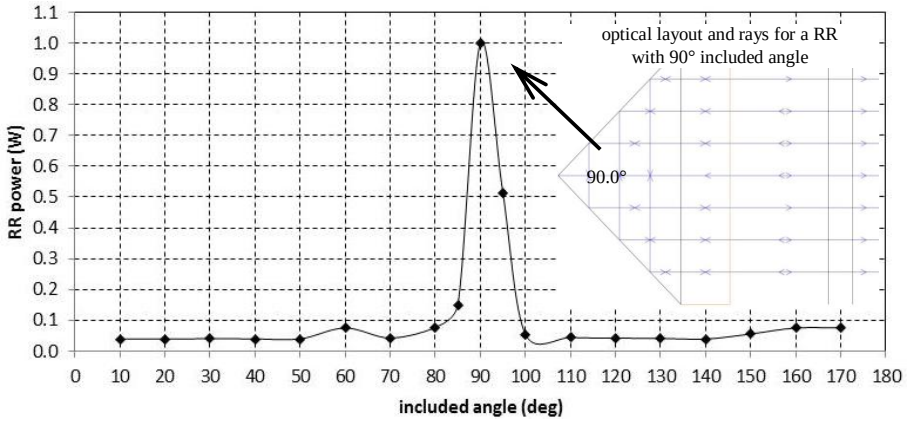

Figure 2.3: Correlation between the optical efficiency of the RR and its included angle

It is also necessary to reemphasize that the TIR associated with IC RRs is caused by uncoated facets. The absence of the metal-coated reflection facets, that is characteristic to other types of RRs, results in cost-effective components capable of repeatable and reliable functionality.

Conventionally, mass fabrication of RRs is a complex process comprised of several steps revolving around injection molding. As such, the optical performance of the RRs is tightly related to quality and accuracy of the master mold used. While newer approaches advocate for ultraprecise machining involving diamond flycutting/ruling or thin shims, state-of-the-art master fabrication continue to rely on traditional pin bundling techniques. According to them, molding of the RR geometry can be performed either directly on the forming ends on the pins or by fabricating an intermediary electroform on which RR will be subsequently molded. The main phases involved in the latter manufacturing path are illustrated in Figure 2.4.

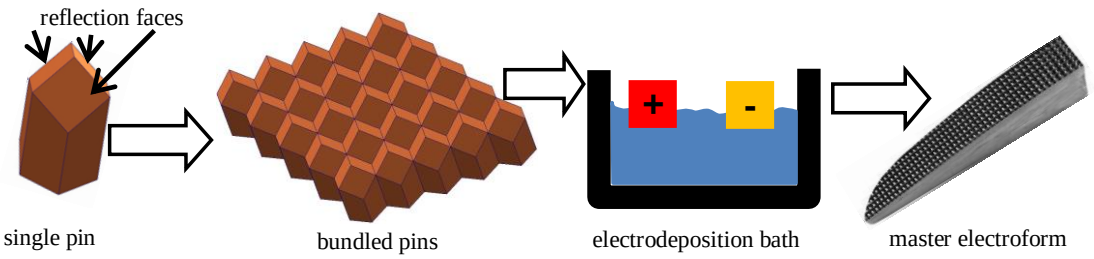

Figure 2.4: Phased fabrication of master electroforms

Typical pins are characterized by hexagonal cross sections and their forming tips have to replicate with high accuracy the "negative" of the intended RR geometry. Because of this, the pins involved in IC RR fabrication are defined by three mutually orthogonal facets. In order to preserve the superior optical performance of the RR, the three retroreflective facets have to meet high optical quality requirements (surface roughness, Ra, < 10 nm) while the angles between cannot deviate by more than 0.05° from the perpendicularity condition. At the next manufacturing step, hexagonal pins are assembled and secured together and their forming ends are then immersed into an electrodeposition bath that allows a continuous

depositing of the nickel atoms. The master electroform that is generated at the end of the process becomes the key component of a core or cavity insert to be integrated in the mold to fabricate the final rear lighting product.

The vast majority of automotive taillights are fabricated from transparent polymeric materials such as polymethyl methacrylate (PMMA), acrylic or polycarbonate. All of these materials are capable of meeting all optical requirements of the RRs, both from safety and illumination perspectives.

Depending on the practical application, automotive lighting generally relies on three typical RR designs: right triangular prism, and CCs with triangular or hexagonal apertures. Their characteristic geometries are illustrated in Figure 2.5.

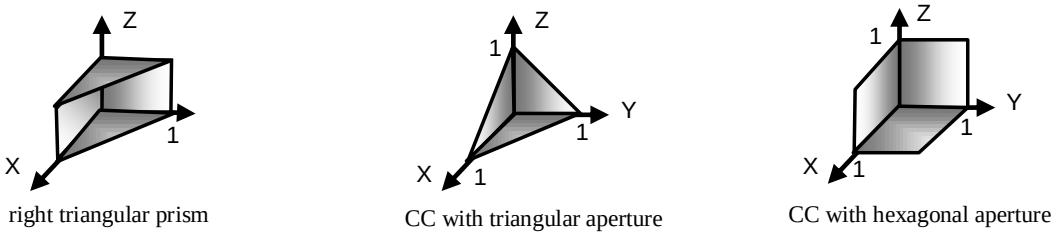

Figure 2.5: Typical RR geometries

The differences between these three designs reside in both the geometry of the elementary RR features as well as the way in which they are positioned and oriented in the overall array forming the structured surface. The optical performance of retroreflective component is tightly related to the reflective area of its facets and it can be characterized by two parameters: i) retroreflection efficiency (RRE); and ii) divergence of the retroreflected light.

Retroreflection efficiency (RRE) is defined as the ratio between the incident and reflected power of the light. It is obvious that while the target RRE is 100%, not the entire area of the RR contributes equally to the TIR phenomenon. Because of this, definitions of retroreflection area (Brinksmeier *et al.*, 2008) and effective aperture (Yuan *et al.*, 2002) were introduced in the optical analysis/design of the RRs. Similar to the direct dependence between RRE and the optical performance, divergence represents – from a pure theoretical standpoint – a desirable safety trait of the RRs since it enhances their visibility by means of a wider observation angle. However, divergence can also be nothing else but a consequence of the manufacturing imperfections translated into angular deviations between the RR facets.

To illustrate this aspect, results from numerical simulations performed by means of Zemax OpticStudio Professional software (Figure 2.6) clearly suggest that an error of ±0.5° between the orthogonal reflection facets does not significantly affect RRE values since almost a 100% RRE is associated with 89.5° and 90.0°, while a 95.55% RRE is determined by a 90.5° angle (Figure 2.6, top row). However, the retroreflective light pattern represented by the incoherent irradiance in W/cm^2 units (Figure 2.6, bottom row) will significantly affect the functionality of the RR, especially its divergence.

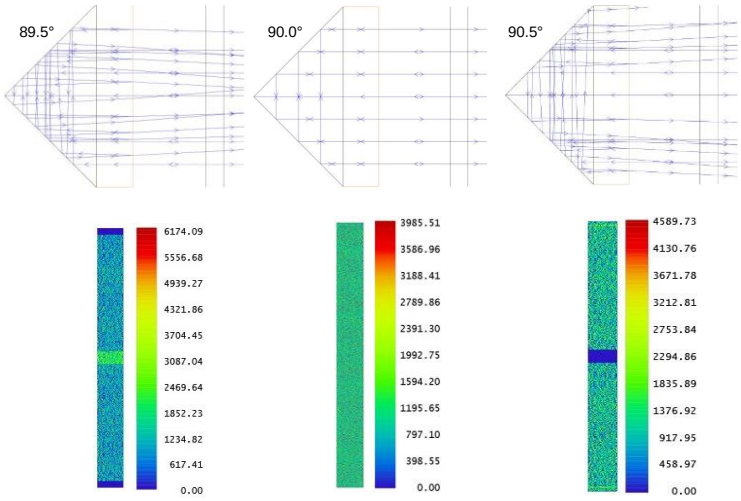

Figure 2.6: The effect of manufacturing defects on the optical performance of the RRs

Clearly, the attainment of the theoretical value of 90.0° for the included angle of a RR will ensure an ideal maximum RRE of 100% coupled with a zero divergence (Figure 2.6, central column). However, as soon as the manufactured included angle departs from its prescribed nominal value, both RRE and divergence will be affected. On one hand, in case of an undersized included angle, some of the incident rays will deviate from their ideal parallel trajectories and will concentrate in the central region of the RR before reaching the observer (Figure 2.6, left column). On the other hand, a significant majority of the incoming rays will diverge outward in case of an oversized included angle, the only exception being constituted by the central rays. While it might appear that the divergence represents an undesirable byproduct of the imperfections that are inherently associated with RR fabrication, it will be reiterated here that in fact a certain amount of divergence is highly desirable in a RR since it is associated with a wider observation angle.

2.4 Parametric Modeling Framework

By taking into consideration the aforementioned typical designs, optical functionalities, and fabrication aspects, it seems that a parametric modeling approach will enable a facile modification of the RR design in an attempt to meet concurrent and sometimes contradictory design constraints. The proposed parametric approach will be able to establish a functional dependence between the input design parameters and the output metrics associated with the optical performance of the RRs, namely RRE and divergence. To illustrate this, the remainder of the study will implement the proposed approach in the context of triangular prismatic RR.

When it comes to the design of an automotive rear lighting component whose elementary RR consists of a right triangular prism, three different types of design parameters can be identified (Figure 2.7).

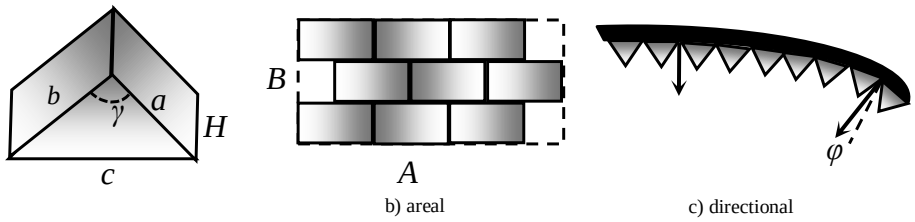

Figure 2.7: Types of parameters controlling the design of automotive rear lighting

As it can be seen in Figure 2.7a, if the two triangular bases of the right prism are right triangles ($\gamma = 90°$) then the geometry of the elementary RR is fully constrained by: the length of the base/hypotenuse (c), the length of the catheti (a, b) and width/height of the prism (H). As such, all other secondary design parameters can be calculated by means of

well-known trigonometric formulas. Therefore, the proposed parametric modeling will assume a, b, c, and H as input parameters that exert a direct influence on the optical performance of the RR:

$$\max\{RRE, divergence\} = f(a,b,c,H) \quad [2.1]$$

In addition to the parameters that are internal to the elementary RR, areal parameters are used to control the pattern in which the base retroreflective elements are positioned and oriented on the structured surface. At this level, both elementary (a, b, c, H) and areal (A, B) parameters have to be included in the optimization of optical performance for a RR.

Finally, a higher (e.g. third) level of directional parametric modeling has to be considered when the elementary RRs are to be located on nonplanar/freeform surfaces, which constitutes in fact the most common instance in automotive lighting. In this case, an orientation angle φ is required to set the orientation of the base RR with respect to the surface normal passing through the point opposing the hypotenuse of the right triangular prism (RTP). Depending on the simplifying assumptions made, the optical analysis can be conducted either in planar or 3D scenarios. Moreover, depending on the particularities of the rear lighting application, it is usually necessary to direct the reflected light upward and toward the eyes of the observer (e.g. the driver of the succeeding car) as the taillights of the preceding vehicle are commonly located below the normal line of sight of the succeeding driver. Lastly, directional orientation plays a foreseeable important role on vertical and horizontal divergence, both with relevance in the traffic safety context.

It is well known that all automotive OEMs invest considerable efforts in making their end products more esthetically appealing while improving the overall aerodynamics of the car. Consequently, all externally mounted fixtures – including taillights – have to maintain their optimal functionality while matching an increasingly complex outer shape of the body. However, it is necessary to emphasize that conventional taillight fabrication techniques relying on pin bundling are faced with serious challenges when used on freeform surfaces alternating between quasi-planar and curved zones such is the case shown in Figure 2.8.

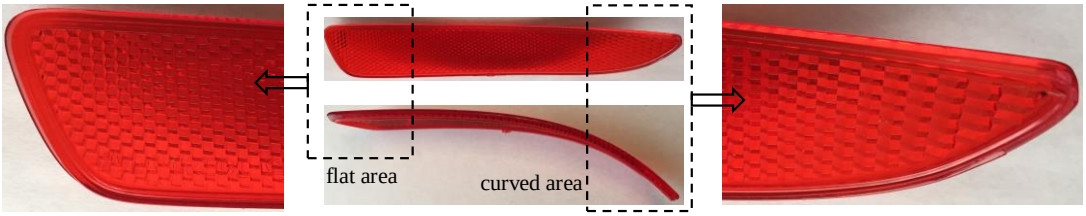

Figure 2.8: Representative sample of an automotive taillight

As it can be noticed from the extreme detail pictures, the geometry of the elementary RR features varies greatly between the quasi-flat and curved zones of the rear light cover. Because of this, significant differences between the forming ends of the pins used on the two primary zones have to exist in order to ensure uniform optical performances across the entire lighting component (Figure 2.9). While alternate fabrication methods could involve tilted pins, their feasibility and reliability have not been tested so far.

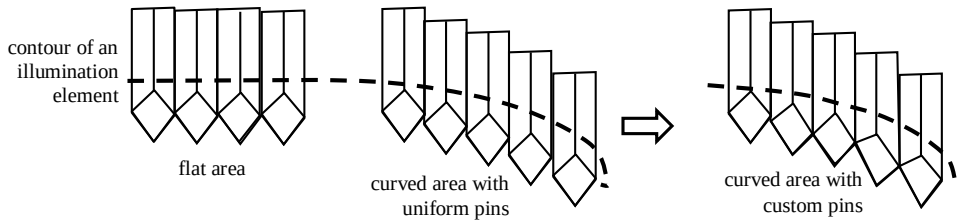

Figure 2.9: Correlation between forming end geometry and ICC RR feature positioning in an array

2.5 Summary and Conclusions

The present study has been centered on the analysis of a particular type of optical components involved in automotive lighting called retroreflectors. While there are three main types of RRs, IC remains the design that is most commonly employed in automotive and safety applications, primarily due to its superior optical performance.

Inverted cube RRs are comprised of two main optical elements that serve simultaneously both illumination and retroflection purposes. On one hand, the illumination element directs the taillight to the surroundings for the purpose of signaling and/or warning. On the other hand, the retroreflective element redirects the light originating from the headlights of a succeeding vehicle back to its driver. This feature is associated with important traffic safety connotations.

Inverted corner cube RRs rely on the TIR phenomenon to redirect incident light in a direction that is opposite and parallel to the incident ray. To be able to efficiently exploit the TIR principles, IC RR has to incorporate one “pass through” facet through which the light both enters and exits, and at least two mutually perpendicular reflection facets on which the light will be totally reflected. Despite the known superiority of IC over other

types of RRs, their overall prototyping and fabrication cost is high (~$2000/in^2 - $3000/in^2) and is associated with long fabrication time (12-14 weeks per electroform).

To address some of the known drawbacks of the merely empirical approach constituting the core of the state-of-the-art technology, a parametric modeling framework capable to generically enclose all typical designs of ICC RRs is proposed. The proposed approach consists of three possible levels for design parametrization (internal, areal and directional) and opens up new investigational avenues in the parameter-driven optimization of the ICC RRs.

Future extensions of this work will be focused on the development of parametrizations for other RR designs, the ongoing goal being to establish a comprehensive platform capable of integrating geometry, optical performance as well as the fabrication of the retroreflective components both at macro and microscale levels.

2.6 Acknowledgments

This paper is the result of collaboration between Western University (London, Ontario) and Canada's National Research Council (London, Ontario). Partial financial support was also provided by Natural Sciences and Engineering Research Council (NSERC) of Canada and AUTO21 Network of Centres of Excellence. Optical simulations were facilitated with the help of CMC Microsystems through the provision of Zemax OpticStudio.

2.7 References

Brinksmeier, E., Gläbe, R. & Flucke, C. 2008. Manufacturing of molds for replication of micro cube corner retroreflectors. *Production Engineering,* **2**, 33-38.

Liepmann, T. W. 1994. How Retroreflectors Bring the Light Back. *Laser Focus World,* **30**, 129-132.

Lloyd, J. 2008. A brief history of retroreflective sign face sheet materials. [Accessed July 24, 2016].

Nilsen, R. B. & Lu, X. J. 2004. Retroreflection technology. *Optics and Photonics for Counterterrorism and Crime Fighting,* **5616**, 47-60.

So, B. S., Jung, Y. H. & Lee, D. W. 2002. Shape design of efficient retroreflective articles. *Journal of Materials Processing Technology,* **130**, 632-640.

Yuan, J., Chang, S., Li, S. & Zhang, Y. 2002. Design and fabrication of micro-cube-corner array retro-reflectors. *Optics Communications,* **209**, 75-83.

CHAPTER 3

Novel Retroreflective Micro-Optical Structure for Automotive Lighting Applications

A version of this chapter was published as: Hussein, S., Hamilton, B., Tutunea-Fatan, O., and Bordatchev, E. 2016. Novel Retroreflective Micro-Optical Structure for Automotive Lighting Applications. *SAE Int. J. Passeng. Cars - Mech. Syst.* **9**(2):497-506, doi:10.4271/2016-01-1407.

3.1 Overview

Retroreflectors (RR) are optical elements that play a critical role in signaling, safety, and aesthetic/styling functionality of automotive lighting. The commonly-used inverted corner cube (ICC) RR structures with hexagonal aperture have several critical limitations that are primarily rooted in their manufacturing technique that involves complex assemblies/shapes of hexagonal pins and electroforms, particularly in case of freeform surfaces. This study introduces a novel RR micro-optical structure, namely: right triangular prism (RTP). The geometric model underlying this new geometry is defined as the intersection between a cube and a plane placed in a particular relative orientation with respect to each other. Following this, non-sequential optical simulation studies were performed using Zemax OpticStudio software. The results obtained by analyzing the incident light orientation have verified the advanced optical functionality of the RTP characterized by a width of 450 µm that is practically unattainable through conventional hexagonal pin-bundling technology. The study also shows that the use of RTPs can overcome the design/optical performance limitations associated with traditional ICC RR designs. Furthermore, the newly-developed single point inverted cutting technology was introduced as a feasible mean to fabricate functional optical prototypes and/or tooling inserts. In this regard, samples of functional RR areas were produced on flat PMMA plates and their preliminary validation has confirmed an increase in the retroreflection efficiency of the RTP compared with conventional ICC RRs. This supports the feasibility and/or potential of RTP as a new RR option for automotive lighting.

3.2 Introduction

Retroreflection is an optical phenomenon that allows the light to be reflected in a direction that is parallel to that of the source (Liepmann, 1994). This optical property is used in a wide range of applications including, but not limited to: metrology, military as well as automotive industry (Liepmann, 1994). By contrast with the wide applicability of RRs, the present study is solely focused on the use of the retroreflectivity in automotive industry, with a particular emphasis on rear and side lighting of the vehicles.

Retroreflection is conventionally achieved by means of passive optical elements called retroreflectors that could be of three main types: lens and mirror, corner cube (CC) and inverted cube (IC). The three main types of ICs defined in Chapter 2 were: right triangular prism (RTP), triangular aperture inverted corner-cube (TA ICC), and hexagonal aperture inverted corner-cube (HA ICC). All three types of IC can be used for tail and side automotive lighting. The IC RR elements used in the automotive industry are usually generated in a variety of plastic without reflective properties. Hence, in order to achieve retroreflection, all ICC RRs rely on a phenomenon known as total internal reflection (TIR) (Kim and Lee, 2007). All IC RR elements share some common geometries in a sense that all IC RR should enclose at least two-three orthogonal reflective facets in order to achieve TIR and thereby retroreflection (Hussein *et al.*, 2015).

This work expands further the development of the IC RR geometries and clarifies how each of those geometries can be obtained from a single unit cube. Further, the present study places a particular emphasis RTP RRs whose possible fabrication methods and optical performance are analyzed in detail. While the optical performance of IC RR could be assessed by means of various criteria such as: retroreflection efficiency (RRE), brightness,

angularity and divergence (Kim and Lee, 2007), the present study has solely focused on RRE as most critical metric for automotive industry.

3.3 Optical Functionality and Geometric Modeling

To fulfill their rear and side lighting functions, the ICC RRs used in automotive industry consist of two elements: i) the retroreflective element with a primary role in safety and ii) the illumination element with role in illumination during signaling, braking, etc. as detailed in Chapter 2. The RRs in the retroreflective tailgate are placed in an array capable to reflect the light back to the succeeding traffic to ensure that the preceding vehicle is visible. On the other hand, the illumination element consists of a generally large slab-like structure that essentially holds individual RRs together in the array. The illumination element allows the passage of the light generated by the preceding vehicle for the purpose of signaling and braking, and positions the individual RRs in a 3D array that matches the external styling of the car. To illustrate these concepts, Figure 3.1 depicts the retroreflective and illumination elements of an ICC RR that belongs to the tailgate.

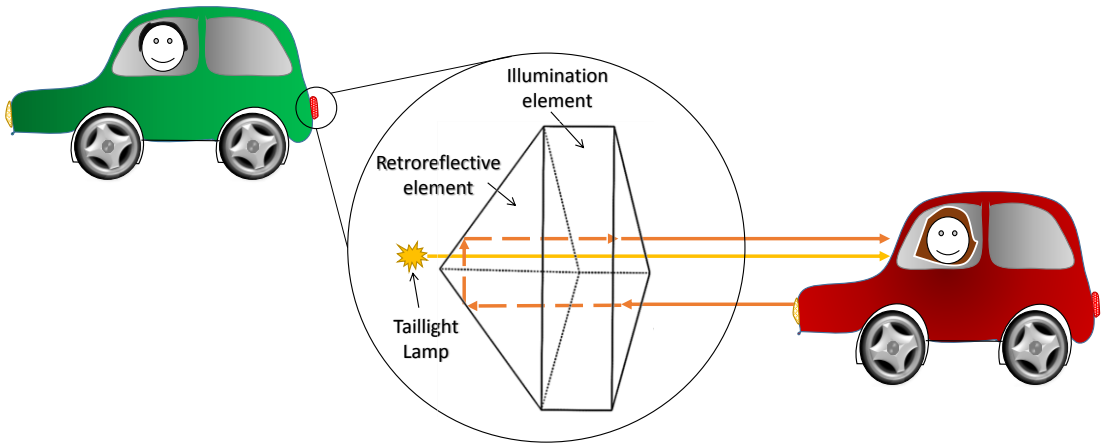

Figure 3.1: Retroreflectors: optical functionality and structure

It is important to note that these two functionalities (illumination and retroreflectivity) do not operate simultaneously and therefore do not optically compete, while the external shape of rear and/or side lighting has to fit the general styling of the vehicle to which they belong to.

To address just its retroreflective function, a typical taillight RR should consist of an incident facet through which light will enter/exit and at least two orthogonal reflective facets capable of successively deviating and then returning the beam in a direction parallel with that of incidence (Figure 3.2). The fascicle of incident/incoming light will first pass through the illumination element and then will access the RR element through its incident facet. After that, the light will hit first and second reflective facets respectively, and they will successively deviate the fascicle according to TIR laws. After the contacting the second reflective facet, the light is redirected to the incident facet and passes again through the illumination element before being released to the environment. Because of the double TIR, the incident and emergent rays are parallel which in fact represents the essence of retroreflectivity.

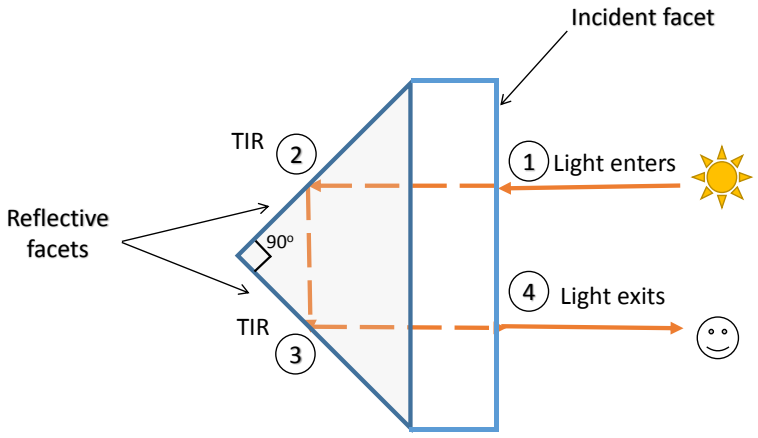

Figure 3.2: Working principle of a typical TIR-based RR element

From a geometrical standpoint, all conventional IC RRs can be generated by means of a cube of a particular orientation that is trimmed off with a plane of a certain position relative to the cube. The retained corner of the cube provides the required retroreflective functionality of the element generated in this manner.

The commonly used in automotive lighting ICC RRs can be modeled as a result of two consecutive geometric transformations/operations (Figure 3.3). Initially, a unit cube is positioned with the bottom-rear-left A vertex at {0, 0, 0} and sides parallel with principal X, Y, and Z axes of the coordinate system. After that, the unit cube is rotated around the vector $\mathbf{n} = \mathbf{Z} \times \mathbf{V}$, with an enclosed 3D angle of $\tan^{-1}(\sqrt{2}) = \theta = 54.74°$, in such a way that the main diagonal of the cube (e.g. **V** or AB direction) becomes vertical.

Vector **n** is then normalized to $\hat{\mathbf{n}}$ and its coordinates are substituted in Equation 3.1 to obtain the rotation matrix **R** with which the cube is rotated 54.74° (Zeid, 2005). The general rotation matrix **R** about an axis with an arbitrary spatial direction is defined as (Zeid, 2005):

$$\mathbf{R} = \begin{bmatrix} n_x^2(1-cos\theta)+cos\theta & n_x n_y(1-cos\theta)-n_z\,sin\theta & n_x n_z(1-cos\theta)+n_y\,sin\theta \\ n_x n_y(1-cos\theta)+n_z\,sin\theta & n_y^2(1-cos\theta)+cos\theta & n_y n_z(1-cos\theta)-n_x\,sin\theta \\ n_x n_z(1-cos\theta)-n_y\,sin\theta & n_y n_z(1-cos\theta)+n_x\,sin\theta & n_z^2(1-cos\theta)+cos\theta \end{bmatrix} \quad [3.1]$$

where n_x, n_y and n_z are the *X*, *Y*, and *Z* components of the normalized vector $\hat{\mathbf{n}}$ respectively, and θ is the 3D angle between the vector **V** and *X*, *Y* or *Z* axes (θ = 54.74°).

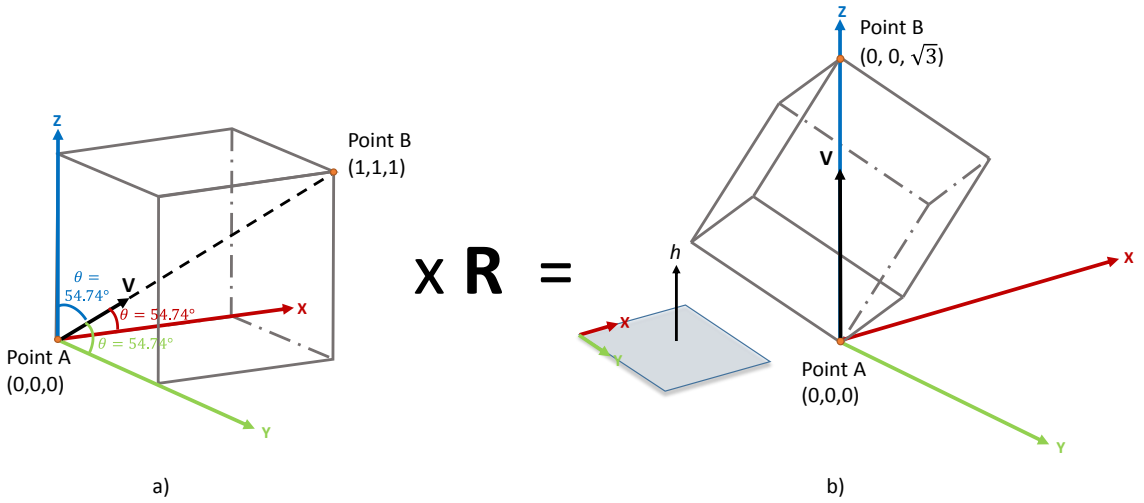

Figure 3.3: Geometrical definition of the ICC RR: a) original unit cube to be rotated with θ about n and b) trimming plane (h || V || k)

This transformation can be described mathematically as:

$$\begin{bmatrix} 0 & 0 & 0 \\ 0 & 1 & 0 \\ 1 & 1 & 0 \\ 1 & 0 & 0 \\ 0 & 0 & 1 \\ 1 & 0 & 1 \\ 0 & 1 & 1 \\ 1 & 1 & 1 \end{bmatrix} \cdot \mathbf{R} = \begin{bmatrix} 0 & 0 & 0 \\ 0.5000 & 0.3659 & 1.1548 \\ -0.2886 & 0.5773 & 0.5774 \\ 0.7886 & -0.2114 & 0.5774 \\ -0.5774 & -0.5774 & 0.5773 \\ 0.2113 & -0.7887 & 1.1547 \\ -0.8660 & 0 & 1.1547 \\ 0 & 0 & 1.7321 \end{bmatrix}, \qquad [3.\ 2]$$

where the initial left term encompasses the coordinates of the 8 vertices of the original unit cube. Following the rotation, the unit cube has to be trimmed off by means of a horizontal plane of normal **h** (**h** ‖ **V** ‖ **k**) that can be positioned at variable distances *h*, $h \in [0, \sqrt{3}]$ between A and B (Figure 3.3b) to form ICC RRs with different apertures. As Table 3.1 shows, the shape of the aperture is strongly dependent on the location of the trimming plane (*a* represents the side of the cube).

Table 3.1: Dependence between ICC RR aperture geometry and trimming plane location

Aperture Shape	Cutting Plane Height
Triangular	$0 < h \le a\frac{\sqrt{2}}{2}\sin\theta$
Enneagonal	$a\frac{\sqrt{2}}{2}\sin\theta < h \le a\left(\sqrt{3} - \frac{\sqrt{2}}{2}\sin\theta\right)$
Hexagonal	$a\left(\sqrt{3} - \frac{\sqrt{2}}{2}\sin\theta\right) < h < a\sqrt{3}$

The aperture of each of the three elements is primarily defined by the number of sides (Figure 3.4)

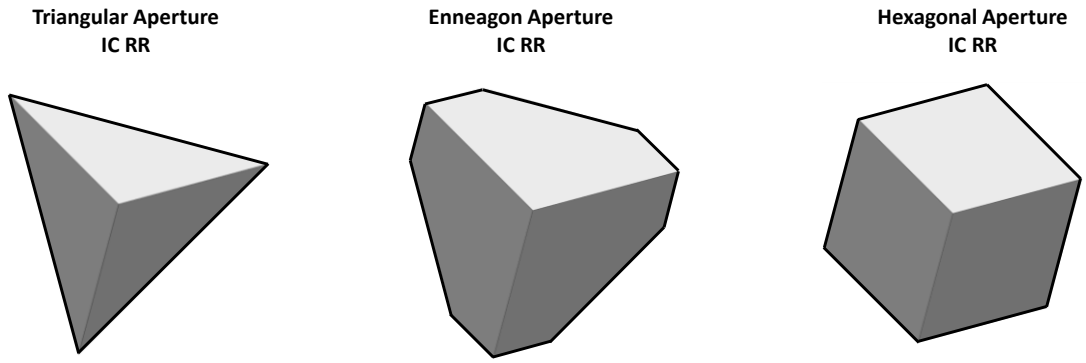

Figure 3.4: Top view of the three main ICC RR

As discussed above, the retroreflectivity of all IC retroreflective elements stems in the mutual orthogonality of their internal reflective faces as well as the TIR phenomenon. Because of this, a new design option for RRs could involve a right triangular prism (RTP) to be formed by two geometrical transformations of the unit cube: i) -45° rotation around

X-axis to be followed by ii) scaling the length along Y-axis. These transformations are depicted in Figure 3.5, where $\mathbf{R}_X$ is the rotation matrix about the X-axis and $\mathbf{S}_X$ is the scaling matrix in the X-axis. Equations 3.3 and 3.4 show the rotation matrix about X-axis and the scaling matrix in the X-axis, respectively.

$$\mathbf{R}_X = \begin{bmatrix} 1 & 0 & 0 \\ 0 & \cos\beta & -\sin\beta \\ 0 & \sin\beta & \cos\beta \end{bmatrix}, \qquad [3.3]$$

where β = -45°, and

$$\mathbf{S}_X = \begin{bmatrix} s_x & 0 & 0 \\ 0 & 0 & 0 \\ 0 & 0 & 0 \end{bmatrix}, \qquad [3.4]$$

where s_x is the scaling coefficient by which the rotated cube could be enlarged ($s_x > 1$) or shrunk ($s_x < 1$), as required.

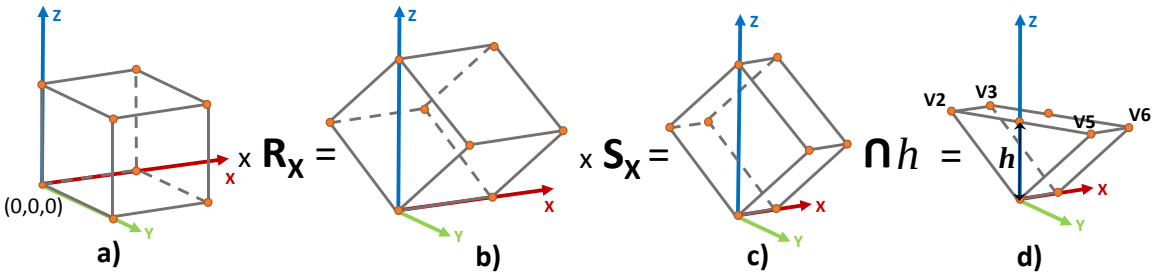

Figure 3.5: Geometrical definition of the RTP: a) original unit cube; b) rotation with β around *X*-axis; c) scaling along *X* axis and d) horizontal trimming of the unit cube

These transformations can be modeled as:

$$\begin{bmatrix} 0 & 0 & 0 \\ 0 & 1 & 0 \\ 1 & 1 & 0 \\ 1 & 0 & 0 \\ 0 & 0 & 1 \\ 1 & 0 & 1 \\ 0 & 1 & 1 \\ 1 & 1 & 1 \end{bmatrix} \times \mathbf{R}_X = \begin{bmatrix} 0 & 0 & 0 \\ 0 & 0.7071 & 0.7071 \\ 1 & 0.7071 & 0.7071 \\ 1 & 0 & 0 \\ 0 & -0.7071 & 0.7071 \\ 1 & -0.7071 & 0.7071 \\ 0 & 1 & 1.4142 \\ 1 & 1 & 1.4142 \end{bmatrix} \times \mathbf{S}_X = \begin{bmatrix} 0 & 0 & 0 \\ 0 & 0.7071 & 0.7071 \\ s_x & 0.7071 & 0.7071 \\ s_x & 0 & 0 \\ 0 & -0.7071 & 0.7071 \\ s_x & -0.7071 & 0.7071 \\ 0 & 1 & 1.4142 \\ s_x & 1 & 1.4142 \end{bmatrix} \cap h = \begin{bmatrix} 0 & 0 & 0 \\ 0 & 0.7071 & 0.7071 \\ s_x & 0.7071 & 0.7071 \\ s_x & 0 & 0 \\ 0 & -0.7071 & 0.7071 \\ s_x & -0.7071 & 0.7071 \\ 0 & 1 & 0.7071 \\ s_x & 1 & 0.7071 \end{bmatrix}, \quad [3.5]$$

where the initial left term represents the matrix of vertices for the original unit cube. After rotation and scaling are completed – same as for ICC RRs – a horizontal trimming plane can be used to generate the final RTP geometry, as illustrated in Figure 3.5d. It is important to recognize that the added scaling enables the dimensional decoupling of the two sides of rectangular aperture of the RTP that would be dependent in absence of the scaling transformation. Also, while the trimming plane could be positioned virtually anywhere below the middle of the rotated cube ($0 < h < \frac{a\sqrt{2}}{2}$), it was assumed, for simplicity reasons, that $h = \frac{a\sqrt{2}}{2}$.

3.4 Optical Simulation and Analysis of Prismatic RR Micro-Optics

As it was found in Chapter 2, RTP is characterized by a retroreflection efficiency (RRE) of almost 100% that is attained when the incoming beam enters the element at a 0° incidence angle (*i.e.* perpendicular to the plane of the aperture). However, when the angle of incidence deviates from 0°, both RRE and distribution of the retroreflected light are

completely altered. To further analyze this, a single RTP element was optically modeled and three different scenarios were investigated:

1) RTP without illumination element

2) RTP preceded by a 100 µm thick illumination element

3) RTP preceded by a 1000 µm thick illumination element

Figure 3.6 illustrates the three singular RTP elements that were used in each of the three scenarios. It is important to note that the length of the illumination element was intentionally made considerably larger than that of the aperture of the RTP in order to better mimic the taillight retroreflective elements in which an array of small RTPs would be mounted on a single larger illumination element.

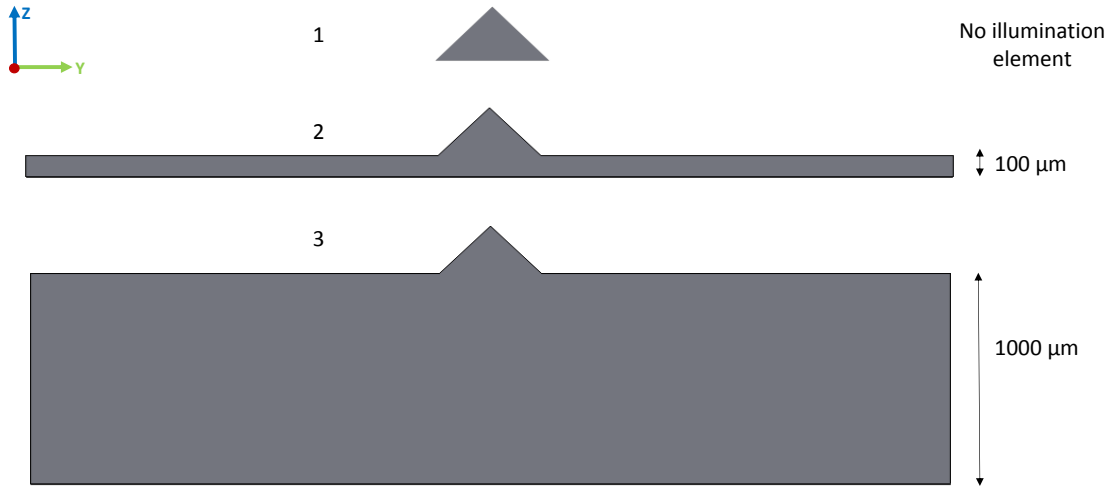

Figure 3.6: Front view of the three analyzed RTP geometries

Optical simulations were conducted to determine the RRE of the three RTPs as the angle of incidence was changed from 0° to 45° in 5° increments. All numerical simulations

involved 10^6 rays and a 100 W power at the light source in an attempt to replicate as close as possible full scale automotive applications setup. The square aperture was dimensioned at 450 µm by 450 µm, and the RR was characterized by a right isosceles triangular shape with $\gamma = 90°$ and $\beta = 45°$ (Figure 3.7).

Also importantly, the position of the light source was continuously adjusted to ensure an adequate intersection between the incident light and the RR in a sense that regardless of the value of the incident angle, the same amount/power of light has entered the RTP through its rectangular aperture. It is relatively easy to imagine that the absence of this provision would have translated into progressively smaller amounts of incoming light to enter the RTP as the incident angle increases.

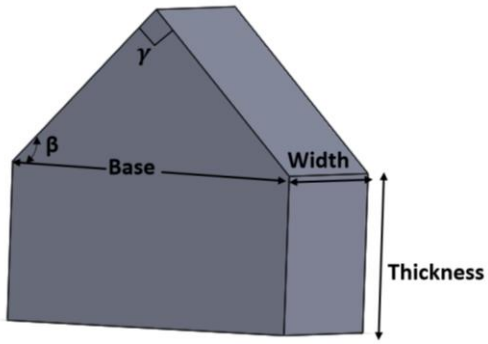

Figure 3.7: Geometric parameters of the right triangular prism

Two important assumptions have governed all optical simulations. First, any ray of light that was reflected, retroreflected or deviated towards the detector (*i.e.* "received light") was regarded as output power as long as it has reached the detector (Figure 3.8). By contrast, any ray that has passed through the RTP element and/or was deviated towards the inside

of the vehicle (*i.e.* has not passed a second time through the illumination element since it was not returned towards it) was regarded as “lost light”.

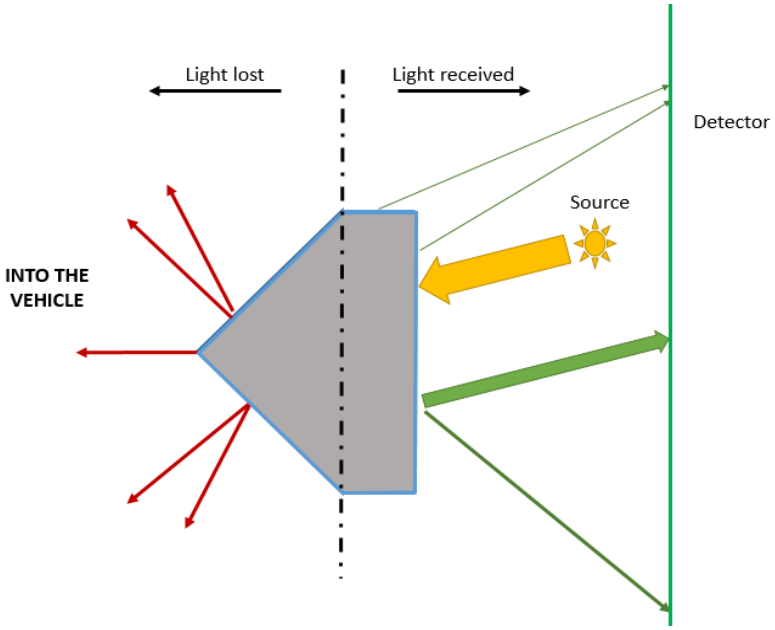

Figure 3.8: Received versus lost light in RTP retroreflector

The configuration of the optical software that underlies the three analyzed scenarios is depicted in Figure 3.9. According to this setup, the source shoots towards RTP rays at desired incident angles and the detector compiles the output of the RR element. The detector has to be sufficiently large to capture all emergent rays that could deviate significantly from the incident direction, particularly in case of large angles of incidence.

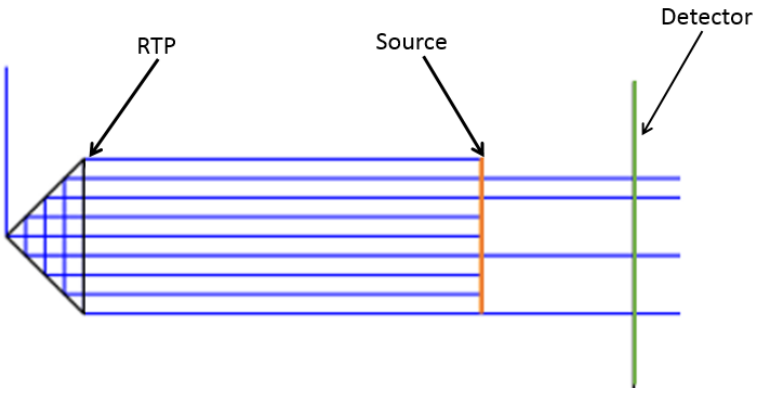

Figure 3.9: Optical software setup

As shown in Figure 3.10, all three scenarios are characterized by a near ideal 100% RRE at 0° incidence angle, which then decreases to almost null values as the angle of incidence increases. This happens because at larger incident angles, more and more of the incident beams start to escape from the RTP in an undesirable direction. In optical terms, this simply means that light rays intersect reflective facets at angles smaller than the critical value and this in turn prevents the occurrence of TIR. Furthermore, the illumination element seems to have a slightly negative effect by further decreasing the output power by contrast with the “no illumination” baseline.

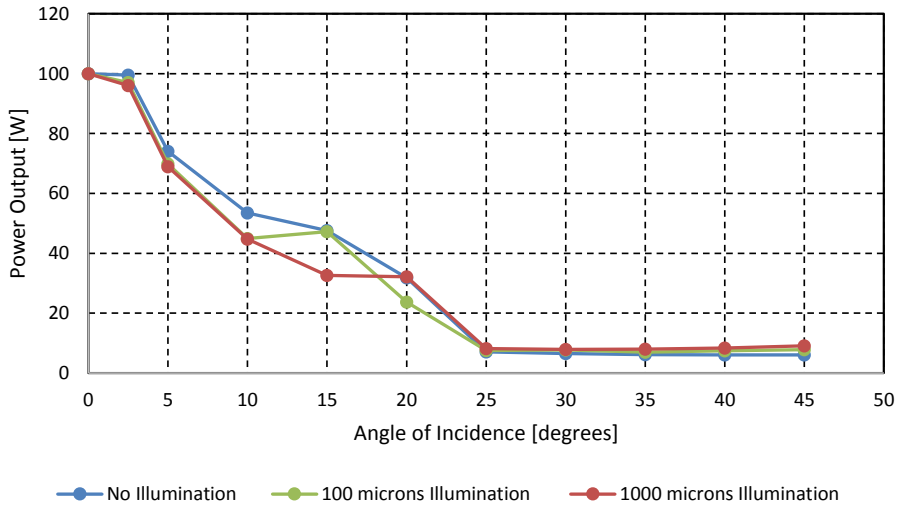

Figure 3.10: The relationship between the incidence angle and output power

In addition to the overall power output, from a practical perspective, it would be interesting to know whether the retroreflected light is being returned in a direction close to that of the light source or elsewhere. Based on this, the light received by the detector was divided into two components, namely "retroreflected" (*i.e.* potentially useful) and "reflected" (*i.e.* potentially useless) light. As illustrated in Figure 3.11, retroreflected light is being returned towards the source, whereas reflected light is being returned away from the source, the boundary between them being drawn by the zero incident angle position.

While it is tempting to associate the retroreflected light with a useful return direction and the reflected light with a quasi-lost power, it will be reminded here that while it is true that in common automotive applications the position of the light source and that of the observer (*i.e.* succeeding driver) are confounded, this is usually not the case for traffic safety applications in which the incident light should be dispersed at angles as wide as possible in order to elevate the nocturnal visibility of the roadside traffic signs, for instance.

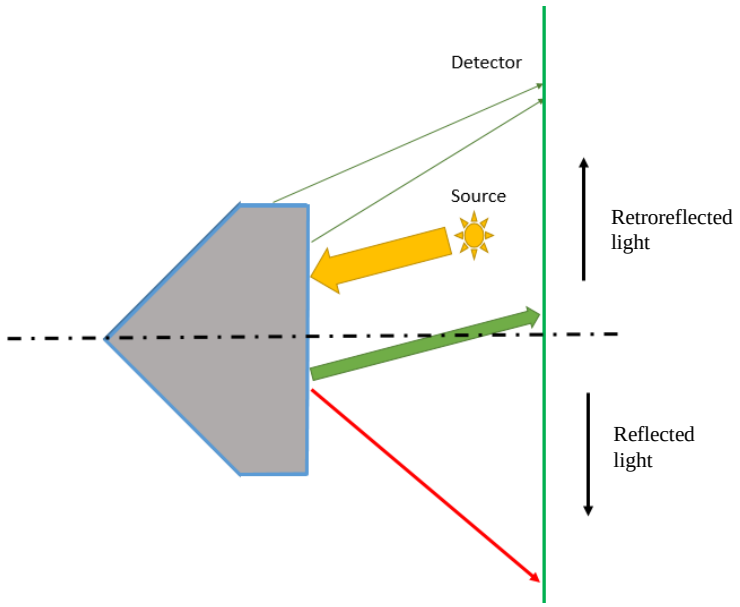

Figure 3.11: Retroreflected versus reflected power output

The results summarizing the split between retroreflected and reflected components of the light is presented in Figures 3.12 – 3.14. All three RTPs were characterized by higher retroreflection at incidence angles below 7° and higher reflection above that threshold.

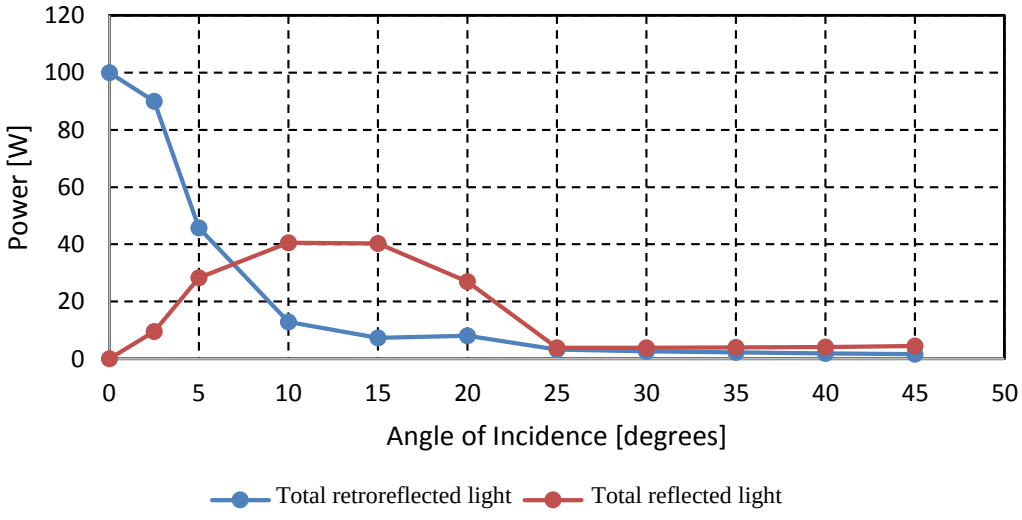

Figure 3.12: Retroreflected and reflected power for scenario 1

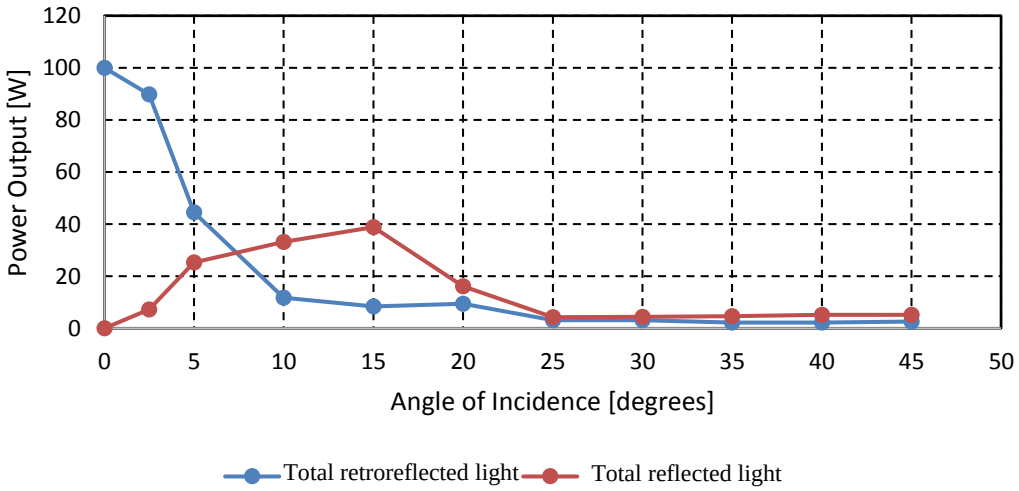

Figure 3.13: Retroreflected and reflected power for scenario 2

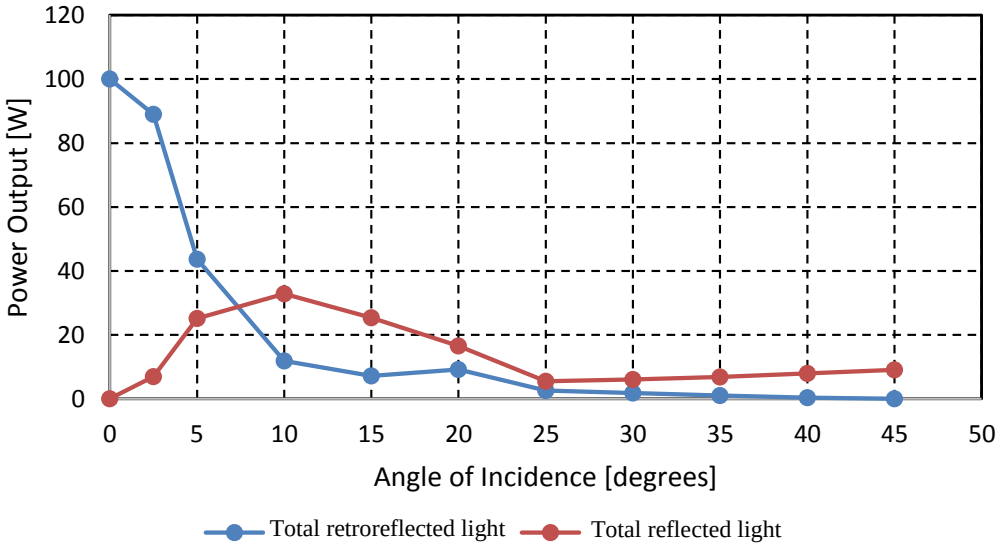

Figure 3.14: Retroreflected and reflected retroreflection for scenario 3

The comparative analysis of the retroreflection for the three retroreflective scenarios reveals that a minimal difference exists between them (Figure 3.15). As such, it can be inferred that while the presence and the thickness illumination element plays an active role

on the overall power output of the RTP, its effect on the retroreflected light is in fact negligible.

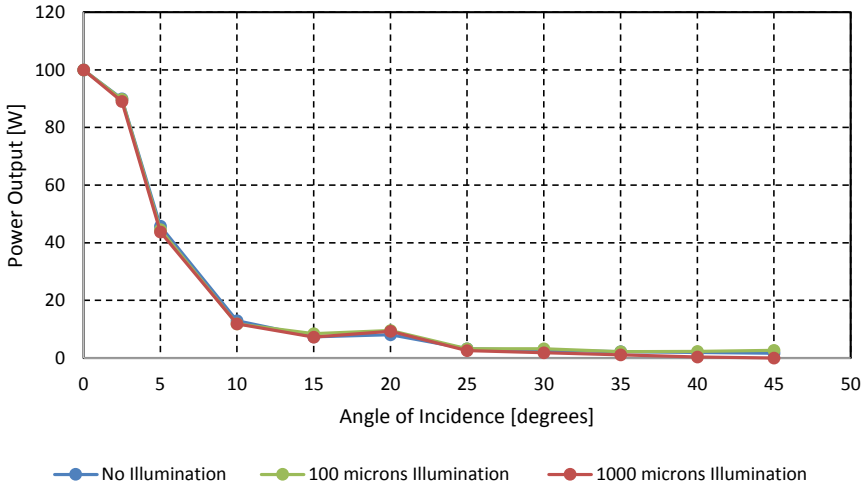

Figure 3.15: Comparative analysis of the retroreflected light

3.5 Conventional Fabrication of Automotive Retroreflective Optics

Retroreflective elements integrated in automotive side and rear lightings are generally fabricated through injection molding. Typical materials used for these components are polymethyl methacrylate (PMMA), acrylic or polycarbonate. The master molds to be used in the RR fabrication process are produced through three main methods, namely: direct cutting, pin bundling and laminating techniques (Brinksmeier *et al.*, 2008). However, the present study will solely focus on the differences between the conventional pin-bundling technique and the newly developed direct cutting, especially since laminating methods are characterized by severe limitations with respect to workpiece geometry, the depth of optical features, surface roughness as well accuracy (Brinksmeier *et al.*, 2008). The geometry used to illustrate the differences between the two aforementioned fabrication techniques will be that of the proposed RTP retroreflectors.

The master mold involved in the serial fabrication of the RRs is in fact an electroform produced through the replication of a stack of pins. For this purpose, individual metal pins with ground and polished tips are bundled together in the orientation and shape that is dictated by the geometry of the final workpiece (e.g. the actual automotive lighting part). After the array of pins is assembled together, the bundle is then inserted in an electroforming bath to form a replica of the active surface/tip of the pins. This replica constitutes in fact the master mold for the RRs belonging to rear and side lightings. Figure 3.16 summarizes the entire process of RR fabrication by means of the conventional pin-bundling technology. It is important to note that the mold formed by the active surface of the pins represents the back side of the retroreflective elements in a taillight and therefore only the negative side of the mold has a direct role in retroreflection.

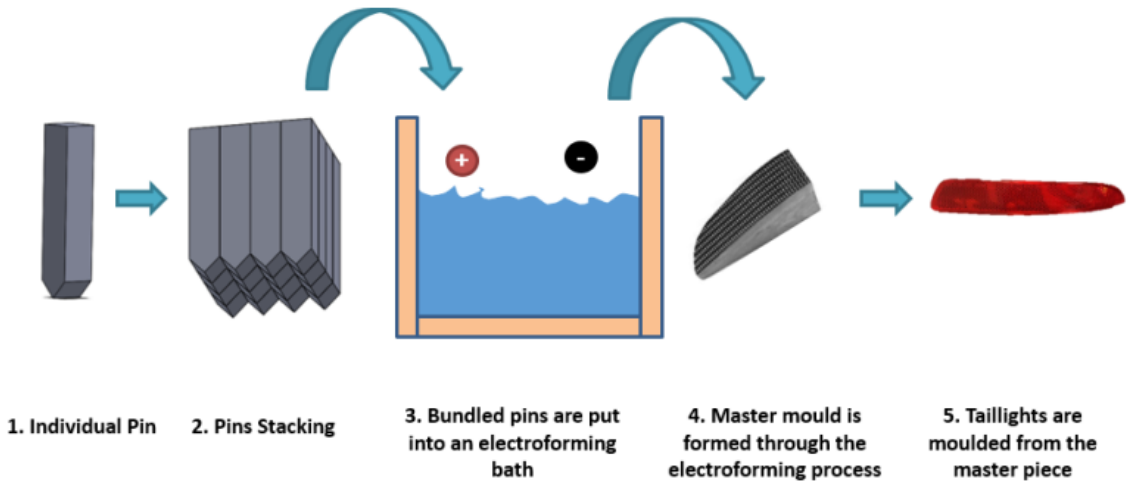

Figure 3.16: Generation of RR elements by means of the conventional pin-bundling technology

3.6 Limitations of Conventional Fabrication Methods in RTP Fabrication

It is relatively easy to anticipate that conventional pin-bundling techniques can be used to generate the newly-proposed RTP geometry (Figure 3.18).

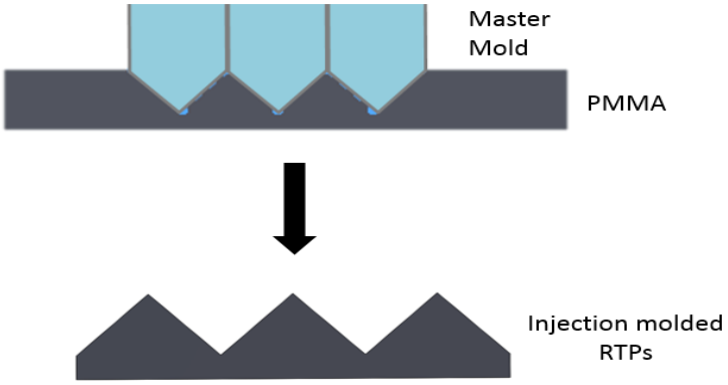

Figure 3.17: Fabrication of RTPs by means of pin-bundling technology

However, as indicated earlier, tail and side lightings are to match the aerodynamic shape as well as the overall styling of the vehicle to which they belong. As such, most automotive lighting elements are not placed on planar surfaces but rather on complex/freeform ones, and in this case the conventional pin-bundling can only offer suboptimal manufacturing solutions.

Indeed, if pin-bundling technology would be used to generate RTP structures on non-planar surfaces, it would be reasonable to expect the formation of certain pocket-like structures (Figure 3.18). Their presence is nothing but an expression of the impossibility to adequately control the shape of the replicate geometry to be formed on the mold master side, particularly when the depth at which the pins are being inserted varies continuously due to the changing curvatures of the outer surface of the lighting element.

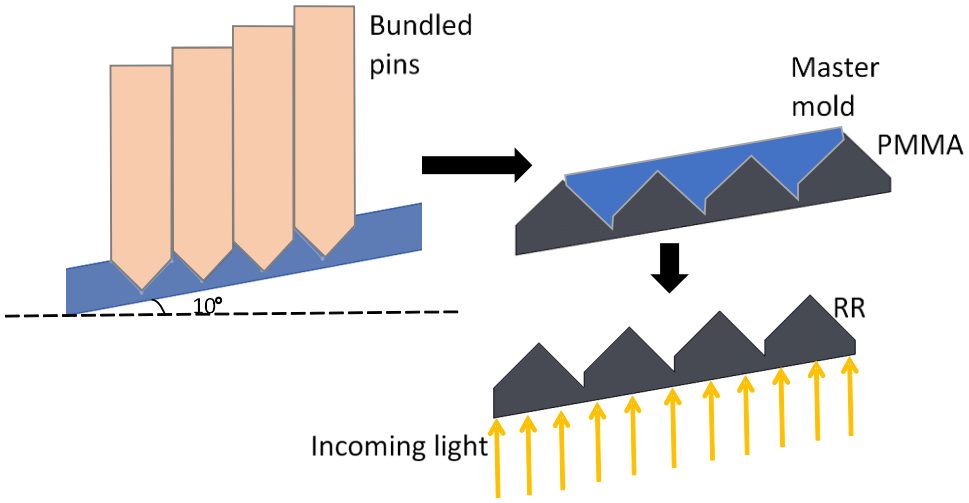

Figure 3.18: Pocket-like structures associated with conventional fabrication of RTPs on non-planar and/or inclined surfaces

Undesirable pocket-like structures are also identifiable in Figure 3.19, as part of a physical taillight featuring conventionally-manufactured ICC RRs.

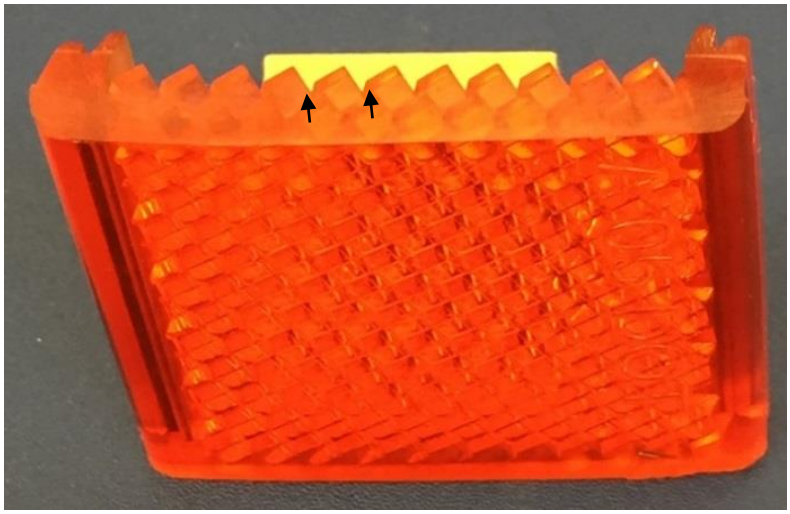

Figure 3.19: Representative cross-section through an automotive taillight

The presence of pocket-like structures represents a significant departure from the

theoretical/idealized “pocket-less” shape of the RTPs fabricated on a non-planar and/or inclined surface (Figure 3.20).

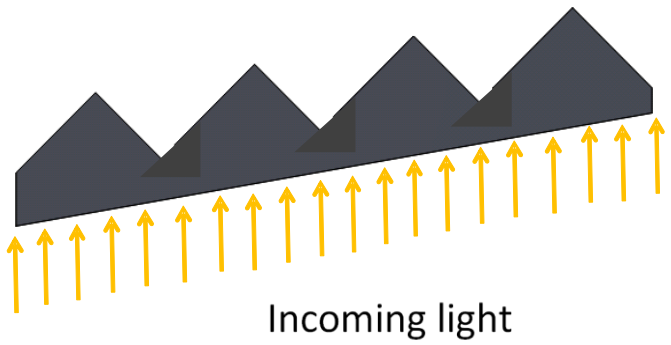

Figure 3.20: Theoretical pocket-less RTP geometry for inclined surfaces

To assess the effect of those structures on the optical performance of the RTPs, a comparative analysis was performed between a manufacturing-feasible array exhibiting pocket-like structures and an idealized “pocket-free” baseline. The optical simulation setup included the two RTP arrays (each placed on 10° inclined slopes), a 1 W light source casting rays at 0° incidence angle with respect to the retroreflective array, $5 \cdot 10^5$ rays, and a detector (Figure 3.21). The null incidence angle was specifically chosen to eliminate any possible bias/confounding yielded from the angled direction of the incident beam.

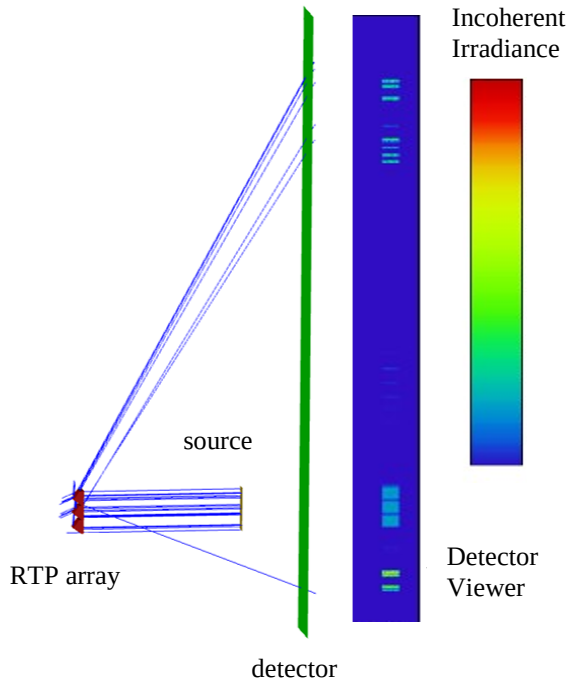

Figure 3.21: Optical setup used to assess the performance of the pocket-like manufacturing imperfections

The retroreflection efficiency (RRE) of each of the two analyzed arrays was calculated as:

$$\text{RRE} = \frac{\text{Reflected Light}}{\text{Incident Light}} \qquad [3.6]$$

Based on this definition, the manufacturing-feasible array exhibited an RRE of 27.7% which is equivalent with a 0.277 W reading at the detector. Further to this, the majority of the retroreflected light was in the "negative" domain meaning that it did not return to the source. Even more interestingly, most of the light that was reflected back to the source was in fact the byproduct of the pocket-like structures that became de facto retroreflectors in this case. The remainder of 72.3% was simply "lost light" as defined earlier in Figure 3.8.

By contrast, the theoretical/idealized pocket-less array analyzed by means of a similar setup (Figure 3.22) has yielded completely different results. In this case, the detector measured an RRE of approximately 100 %, which was in fact consistent with the results obtained in a previous study (Liepmann, 1994). As such, it becomes clear that the presence of the pocket-like structures to be generated through conventional pin-bundling techniques would translate into significant decreases in the optical performance (i.e. RRE) of the RTPs.

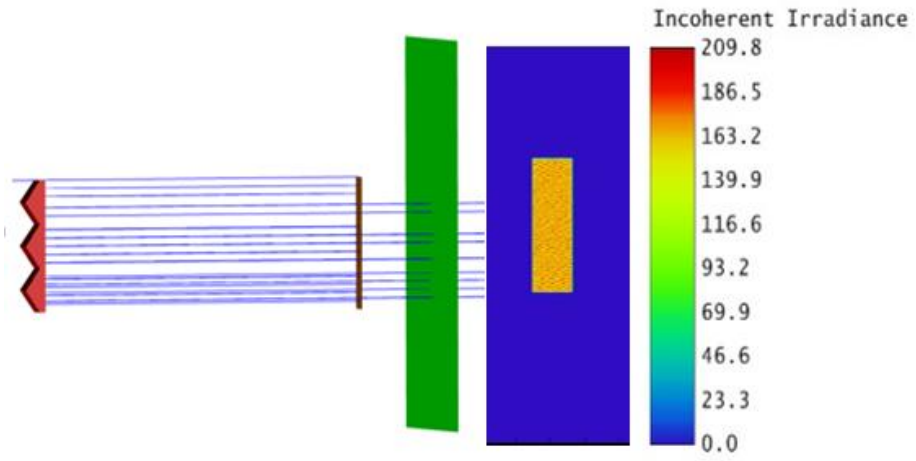

Figure 3.22: Optical setup used to assess the performance of the theoretical pocket-less structures

Furthermore, pocket-like manufacturing imperfections tend to scatter the light in at least 4 different directions, whereas the theoretical pocket-less structure will return all incident light back to the source (Figure 3.23). Both scenarios were carried out with the same 10° inclined assumption for the base surface.

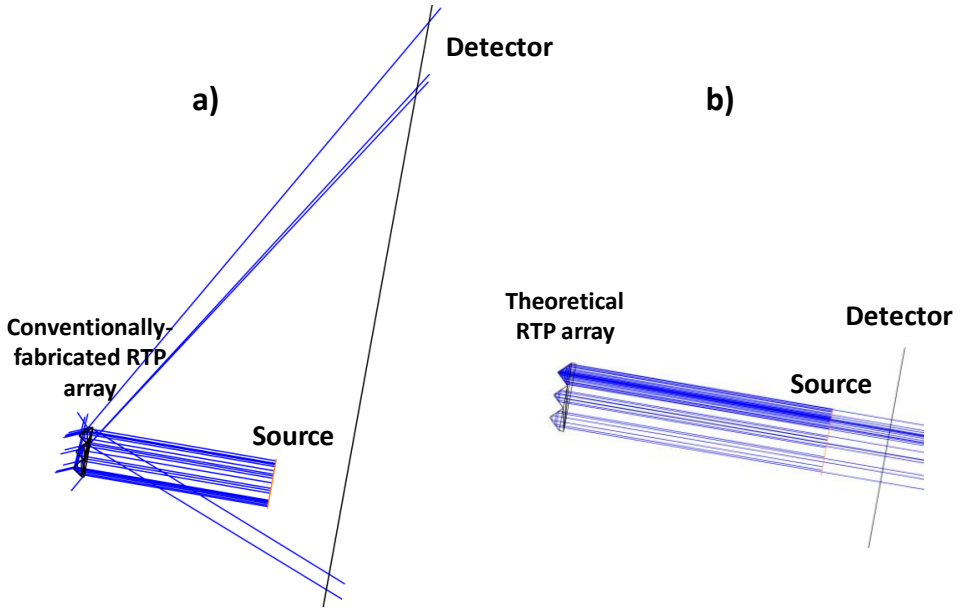

Figure 3.23: Scattering/non-scattering effects associated with: a) conventionally fabricated RTPs and b) theoretical RTPs

3.7 Single Point Inverted Cutting in RTP Fabrication

In an effort to eliminate the aforementioned pocket-like features associated with pin-bundling technologies, alternate manufacturing procedures have been developed. According to (Brinksmeier *et al.*, 2012a; Hamilton *et al.*, 2015), an instance of ultraprecise machining/cutting can be used to machine the desired retroreflective features directly into the raw stock. In addition to the fact that optical surface quality (*e.g.* $R_a < 10$ nm) is absolutely attainable, scalability of the geometry to be fabricated is also possible. In other words, most of the pin-bundling restrictions with respect to the minimal size of the RR microfeatures that can be produced – essentially set by certain pin sizing limits - are no longer a concern when multi-axis cutting is used.

As the name implies, ultraprecise machining relies on a monocrystalline diamond as the cutting tool. In brief, single point inverted cutting is a diamond turning operation "upgraded" with kinematics that is specific to five-axis machining. As (Brinksmeier et al., 2012a) indicates, the novel material removal operation resembles chiseling in a sense that a single point cutting tool is in fact used to remove material in an interrupted cutting motion (Figure 3.24). The two rotary axes of the machine enable proper tool posturing (i.e. position and orientation) with respect to the retroreflective facets to be cut, while machine spindle has to be outfitted with a fixture allowing stationary tool positioning. The cutting tool to be used in the inverted cutting could be regarded as a V-shaped turning tool that is used in a different manner than in a conventional turning operation.

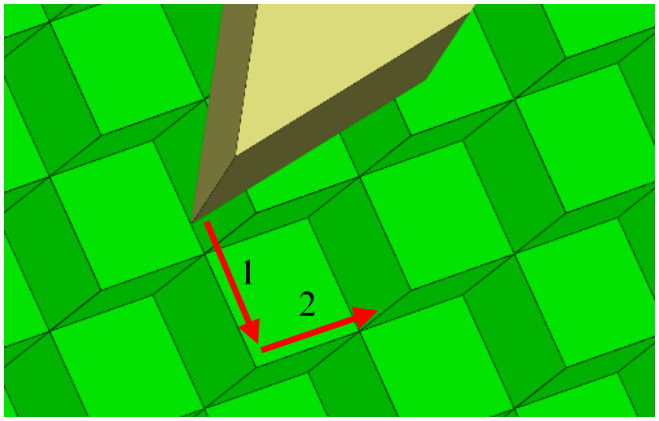

Figure 3.24: Single point inverted cutting kinematics (adopted from (Hamilton *et al.*, 2015))

By assuming that an AC rotary-table five-axis micromachine is used to generate the desired RR microfeatures (A being the primary and C being the secondary rotational axis), the facets of a single traditional ICC structure can be generated one at a time by adequately positioning the two rotary axes, such that – for the duration of the translational primary cut

motion – the facet of the RR feature becomes coplanar with the relief face of the tool. Following this, the tip of the cutting tool is to be directed along the two edges delimiting the facet to be generated (Hamilton *et al.*, 2015). After the first facet has been cut, the C axis has to be rotated 120° in order to expose to the cutting tool to the next facet and the process repeats until a full RR structure has machined. Once a complete RR has been produced, the five-axis machine can then be repositioned to the location of the next microfeature such that a full array could be eventually produced.

By contrast with the conventional ICC RR, the novel prismatic RR proposed in the present study relies on a diamond insert that continue to preserve some of the turning tool characteristics, but at the same time is different than that involved in ICC cutting (Figure 3.25).

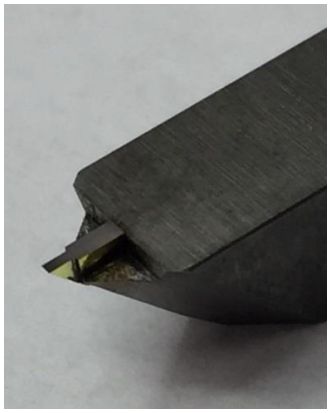

Figure 3.25: Single point inverted cutter for RTP fabrication

Depending on the strategy chosen for the inverse cutting, RTP can be generated either in one or more machining sequences. However, for superior/optical surface quality, both roughing and finishing passes become a necessity. While different cycle cutting strategies can be envisioned, the one described in this study consists of a series of four distinct

motions: two material removal followed by two ancillary (i.e. positioning only) motions, respectively (Figure 3.26). As it can be noticed, the first cutting/plunging motion is a translation along the negative Z-axis direction, while the second/ploughing motion is made along the Y-axis. To limit the amount of load experienced by the tool, material is removed in layers of predetermined thickness, such that the four-motion cycle is repeated until the geometry reaches a near-net shape.

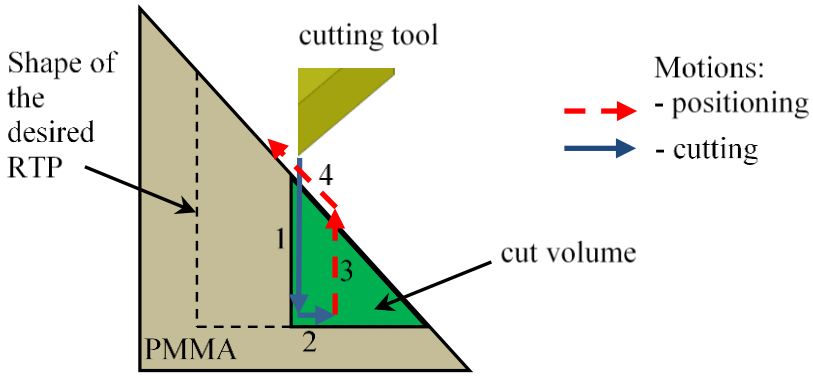

Figure 3.26: Single point inverted cutting kinematics for RTP fabrication

To better illustrate the entire RTP cutting strategy, Figure 3.27 depicts a typical sequence consisting of three distinct phases that are separated by a certain amount of layer thickness that is removed with each plunging motion. As it can be expected, the fundamentally different cutting conditions on two delimiting facets of the RTP will translate into relatively dissimilar surface qualities. More specifically, the positive rake angle associated with the vertical "plunge" should clearly yield a better roughness than that associated with the horizontal "ploughing" in which the rake angle becomes negative (Hamilton *et al.*, 2015).

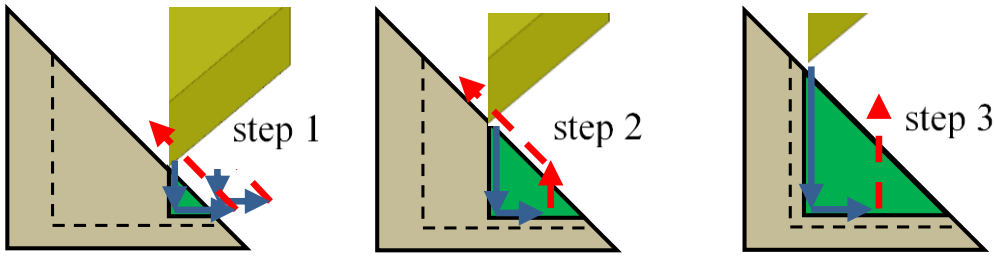

Figure 3.27: Multi-cycle fabrication of RTPs

While the manufacturing sequence described above is performed in a single pass, a two-pass (roughing/finishing) strategy can also be envisioned. In this case, an additional layer of material could be left on the ploughing facet, that would be finished in a subsequent plunging operation to be preceded by a 180° rotation of the workpiece around C-axis.

3.8 Fabrication of the Prototype RTPs

In order to test and validate the proposed manufacturing approach, a functional array of RTPs was generated on a flat PMMA sheet characterized by a 4 mm thickness. Figure 3.28 encloses both overview and detailed views of the RTP array as imaged with a scanning electron microscope. The microfabricated array is composed of 783 RTP elements covering an area of 195 mm^2. With the exception of RR features located on the outer boundary of the array, each RTP is characterized by a square aperture of 450 x 450 μm.

The visual/qualitative analysis of microfabricated RTPs reveals that the fabricated microgeometry replicates closely the targeted geometry. Facets are mutually orthogonal and each apex closely resembles a sharp (*i.e.* “pocket-less”) corner, thereby maximizing the total reflective surface. Since only the single-pass approach was employed in these preliminary cutting trials, the anticipated difference between plunging and ploughing

mechanics translates into fairly notable differences in terms of facet roughness. While the actual cutting mechanism has not been investigated in detail so far, it would be reasonable to predict that while plunging is associated with material shearing and hence a better surface finish, ploughing conditions are associated with material rubbing and therefore a poorer quality of the cut surface.

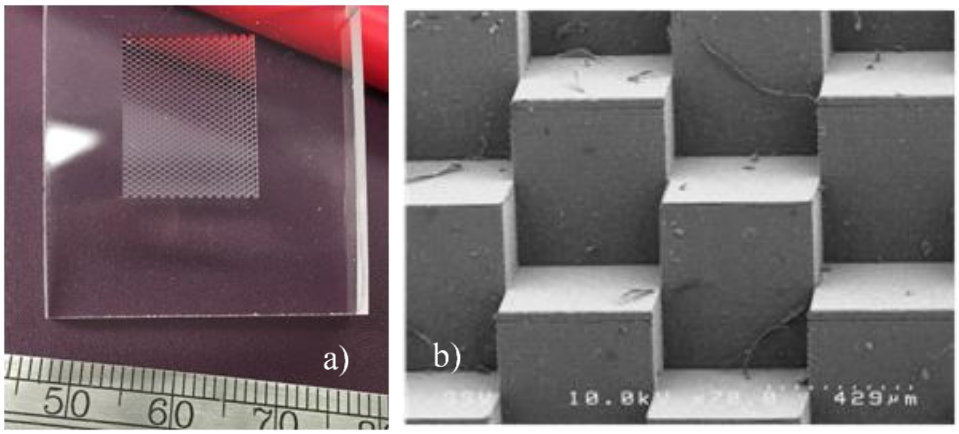

Figure 3.28: Visual aspect of the RTP prototype: a) macroscopic overview and b) detailed SEM imaging

3.9 Experimental Evaluation of Optical Performance of Prismatic RR Micro-Optics

The optical performance of the fabricated RTP prototype was initially evaluated by means of visual appearance followed by an overall assessment of the reflected light power. Both optical comparisons were performed with respect to the conventional ICC RR baseline materialized in the form of typical automotive taillight.

For the purpose of a simple qualitative comparison, the fabricated RTP array was placed in front of a typical ICC retroreflector and both of them were illuminated by white LED light. The results of this comparison are shown in Figure 3.29, where it can be observed

that the microfabricated RTP prototype performs better than the conventionally-fabricated automotive component. Indeed, while the RTP array reflects a significant amount of incident light back to the observer, the automotive retroreflector seems to be characterized by a minimal retroreflectivity. From an application perspective, this increased retroreflectivity means that a lower power source would be required to illuminate an object whose presence is to be signaled by means of RTP RRs, and this would in turn increase the overall nocturnal visibility of the object.

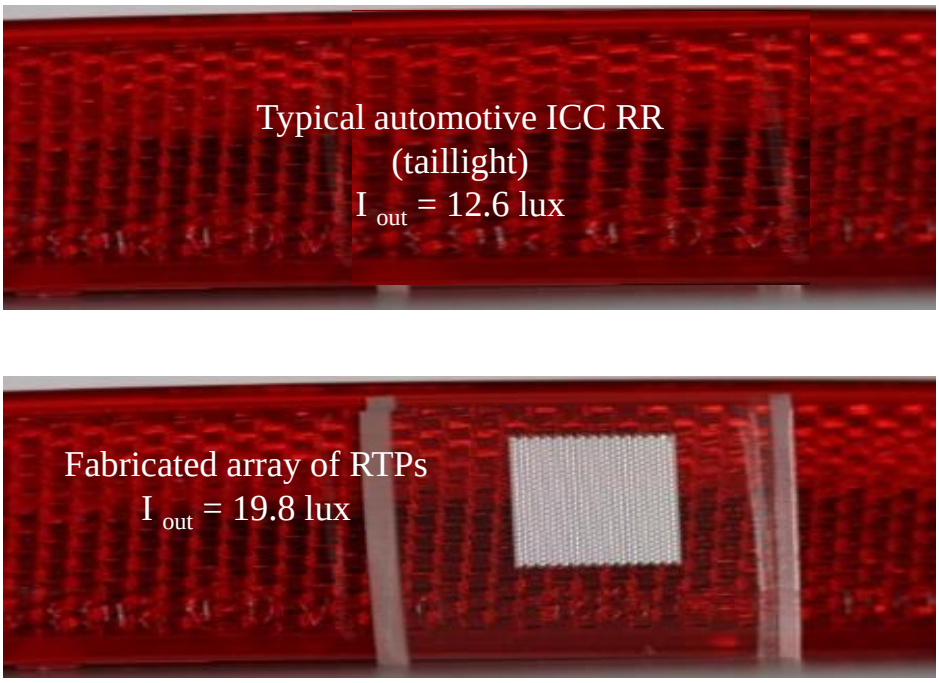

Figure 3.29: Comparative visual/qualitative assessment of the conventional ICC and proposed RTP RR

Furthermore, the optical performance of both ICC and RTP RRs were quantitatively assessed under identical illumination conditions. The experimental setup used to measure their retroreflectivity is shown in Figure 3.30. As it can be noticed, a light source was placed near a digital lux meter detector and they were both 272 mm away from the

retroreflective components. The measurements performed under dark conditions revealed that while the commercial taillight reflects back a power of 12.6 lux, the RTP array prototype returns a power of 19.8 lux.

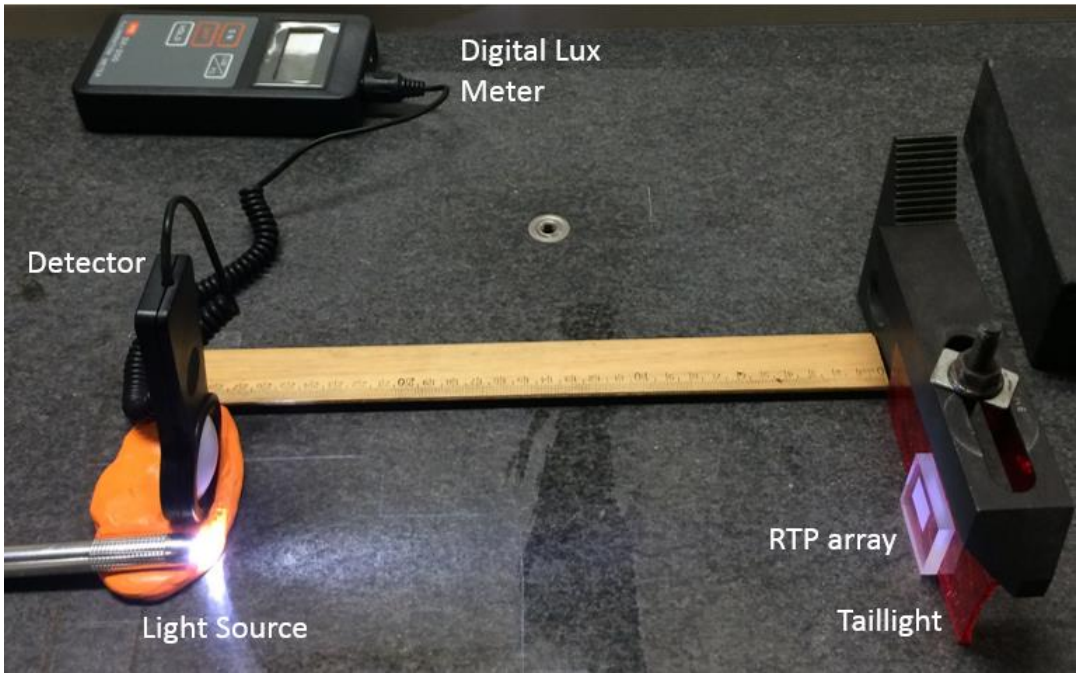

Figure 3.30: Physical setup used to evaluate the retroreflected light

The additional 7.2 lux (57% increase) power suggests that the newly developed RTPs are indeed functional and have comparable retroreflective characteristics to those of conventional ICC RRs. On the other side, it is possible that some measurement inaccuracies were caused by the reflectivity of the non-cut surface around the RTP array such that more precise assessments will be required in the future.

3.10 Summary and Conclusions

A novel retroreflective micro-optical structure was introduced in this study as a possible cost-effective alternative capable of enhancing the performance of the conventional ICC RR elements that are widely and ubiquitously used in automotive lighting.

The design of various IC RR geometries - including RTP - was presented and the optical performance of RTP to be potentially fabricated through both conventional and inverted cutting methods was simulated by means of optical design software. Then, a functional prototype of an RTP array was generated in PMMA through single point inverted cutting performed by means of a diamond tool. Finally, qualitative and quantitative evaluations of both conventional and proposed retroreflective elements were performed for the purpose of comparative assessment of "old" and "new" retroreflective geometries.

Based on all these, the following can be regarded as the main contributions of this work:

1. A unified approach to the geometric modeling of RR elements derived from a unit cube was introduced. The applicability of this approach was then demonstrated in the context of the newly proposed RTP RR geometry.
2. Optical simulations were conducted to assess the retroreflective performance of the RTP with respect to different incidence angles of the incoming light. The results indicate that RRE of the analyzed RTPs decreases as the angle of incidence increases.
3. A possible major drawback of pin-bundling fabrication of RRs on inclined/freeform surfaces is associated with the presence of pocket-like features that act as light traps and thereby significantly diminish the optical performances of the automotive components. These manufacturing-induced

means of inverted cutting that create pocket-less theoretical RTPs and hence restore their full RRE.

4. The physical measurements of the retroreflected light power showed that an RTP array prototype acquired a comparable retroreflective efficiency to the hexagonal ICC ones which suggests that more experiments should be carried out to examine applicability of those RTPs in automotive lighting.
5. Future studies will be focused on advanced spatial optical analysis and more accurate and practical testing and optical performance verification.

3.11 Acknowledgments

This paper is the result of collaboration between Western University (London, Ontario) and Canada's National Research Council (London, Ontario). Partial financial support was also provided by Natural Sciences and Engineering Research Council (NSERC) of Canada and AUTO21 Network of Centres of Excellence. Optical simulations were facilitated with the help of CMC Microsystems through the provision of Zemax OpticStudio.

3.12 References

Brinksmeier, E., Gläbe, R. & Flucke, C. 2008. Manufacturing of molds for replication of micro cube corner retroreflectors. *Production Engineering,* **2**, 33-38.

Brinksmeier, E., Glabe, R. & Schonemann, L. 2012a. Diamond Micro Chiseling of large-scale retroreflective arrays. *Precision Engineering-Journal of the International Societies for Precision Engineering and Nanotechnology,* **36**, 650-657.

Hamilton, B. W., Hussein, S., Tutunea-Fatan, O. R. & Bordatchev, E. V. Strategies in Single Point Inverted Cutting for Fabrication of Structured Surfaces. CANCAM, June 2015 2015. London, Canada: Proceedings of the 25th Canadian Congress of Applied Mechanics, 108-111.

Hussein, S., Hamilton, B., Bordatchev, E. & Tutunea-Fatan, O. R. 2015. Parameter-Driven Geometric Modeling of Retroreflective Features. *CANCAM.* London, Ontario, Canada: Proceedings of the 25th Canadian Congress of Applied Mechanics.

Kim, H. & Lee, B. 2007. Optimal design of retroreflection corner-cube sheets by geometric optics analysis. *Optical Engineering,* **46**.

Liepmann, T. W. 1994. How Retroreflectors Bring the Light Back. *Laser Focus World*, **30**, 129-132.

Zeid, I. 2005. *Mastering CAD/CAM*, McGraw-Hill Higher Education.

CHAPTER 4

Comparative Analysis of Inverted Cube Retroreflectors

A portion of this chapter was published as: Hussein, S., Hamilton, B.W., Bordatchev, E.V., and Tutunea-Fatan, O.R. 2016. Optical Performance of Right Triangular Prism *Proceedings of the Photonics North 2016 Conference*. May 2016, Quebec City, Canada

4.1 Overview

This study is focused on the going through the right triangular prism (RTP) retroreflective geometry product development process in an attempt to examine their optical performance for possible safety applications. In this context, a parametric approach will be developed to form inverted corner cube (ICC) elements and implemented to model RTPs. Moreover, particular emphasis will be placed on the evaluation and comparison of the optical performance of hexagonal aperture (HA) ICCs, triangular aperture (TA) ICCs and RTPs. The optical performance of the retroreflective elements will be assessed through numerical simulations to be performed on both singular as well as arrayed elements. Two main simulation streams were run for the single elements, the first being with a constant reflective area for all retroreflective elements and the second being with constant aperture areas. Results for both simulation sets shows that the novel right triangular prisms (RTPs) are best suited for applications involving low incidence angles, the hexagonal aperture (HA) IC is applicable for areas requiring a medium range of incidence angles, and triangular aperture (TA) IC is the most convenient in high incidence angles demanding applications. RTPs and HAs are finally compared through a physical test using a luminance imaging system in which RTPs show superiority.

4.2 Introduction

Retroreflectors (RRs) are passive optical elements that redirect light to an angle rotated 180° from that of the incident one. They are present in nature such as in a cat's eyes which appear to be illuminated in the dark, and they are used in a wide variety of applications ranging from metrology to automotive (Liepmann, 1994).

There are number of ways for evaluating the optical performance of an RR such as retroreflection efficiency (RRE), effective retroreflective area, range of incidence angles (angularity) and divergence. Different RR types acquire different degrees of those optical properties. However, there are tradeoffs among these performance metrics and it is important to use the correct RR according to the needs of various applications (Kim and Lee, 2007). For instance, RRs used in traffic applications, such as safety signs, require some amount of divergence to make sure the light is retroreflected to the person driving the vehicle rather than the headlights themselves.

There are three main types of RRs: lens and mirror, also known as cat's eye, corner cube (CC) and inverted cube (IC) as listed in Chapter 1. Cat's eye RRs retroreflect light using a lens and a reflective surface, and is most commonly used in road signs and pavements in a form of tiny glass beads (Medicus, 2006). Corner cube (CC) RRs are made of three orthogonal mirrors or reflective metal surfaces and they work by reflecting rays from one mirror to another. They have been used in lunar laser ranging ever since they were planted on the moon during the Apollo mission (Erickson, 2011). ICs, on the other hand, reflect light using total internal reflection (TIR) and they substitute CC RRs in many applications as they have a much higher retroreflection efficiency (RRE) (Yuan *et al.*, 2002; Kim and Lee, 2007). Hence, this study will only focus on IC RRs.

IC RRs are usually made of a transparent material, such as polymethyl methacrylate (PMMA) or acrylic, with a refractive index higher than that of air. When the IC RR facets are hit by rays at incidence angles that are greater than the critical angle, those facets reflect light through TIR among each other to achieve retroreflection (Figure 4.1). They are most commonly seen in automotive safety applications such as tail and side lightings. Two main

types of ICs currently used in the automotive industry are the hexagonal aperture (HA) RR and the triangular aperture (TA) RR, both of which come under a category of ICs called inverted corner cubes (ICCs).

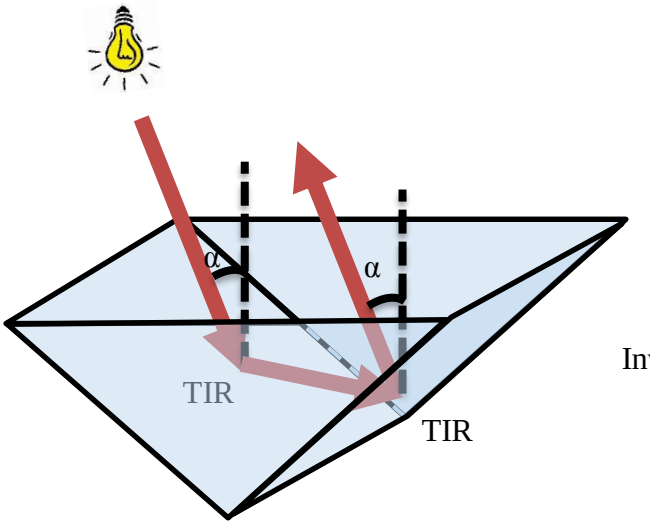

Figure 4.1: Inverted cube retroreflector

In this broader context, a novel IC RR design – termed as right triangular prism (RTP) – will be modeled and then tested (both virtually and physically) in an attempt to determine its optical performance.

Furthermore, this study aims to present a parametric approach to the model the commercial ICC geometries from unit cubes, and implement this approach to model the novel right triangular prism (RTP) IC, that is specially designed for manufacturability (Hamilton *et al.*, 2016a; Hamilton *et al.*, 2016b). Both commercial ICCs and RTP are then tested and their optical performances are compared. The two performance metrics considered in this study are RRE and effective retroreflective area.

4.3 Geometries of Basic Retroreflective Micro-optical elements

As their name indicates, all IC geometries can be deduced from a unit cube. This cube however has to be modified through specific rotation and transformation functions (Zeid, 2005) and then trimmed with a plane to form the required IC geometry. The flow diagram in Figure 4.2 shows the process through which the IC RR is designed from a unit cube, analyzed, fabricated, and tested which follows a typical product development in which design and fabrication are driven by the required optical performance.

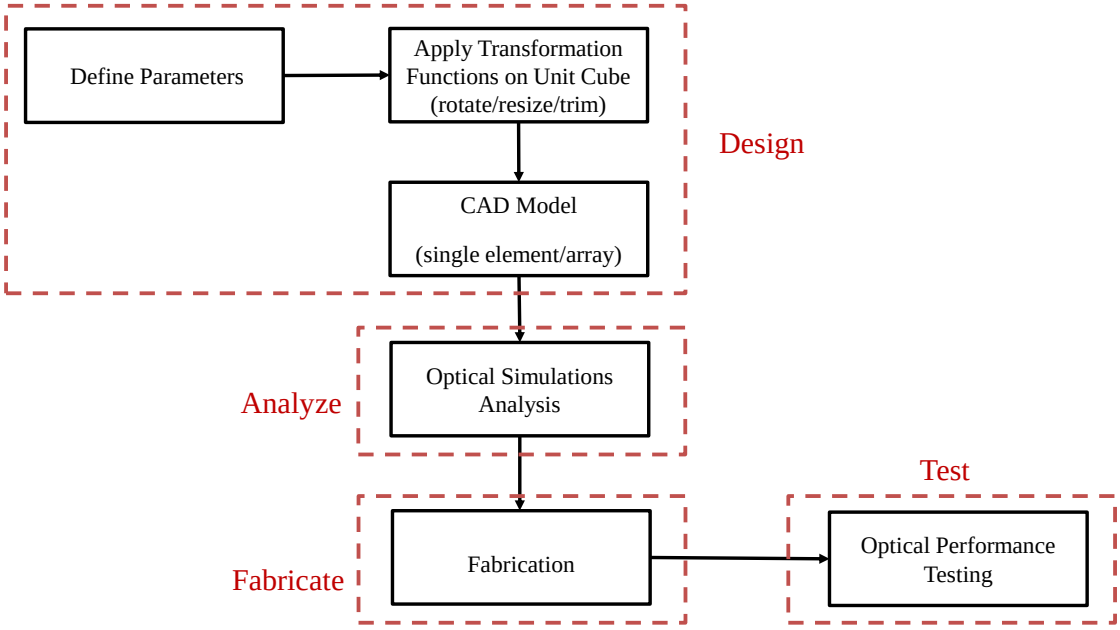

Figure 4.2: Study methodology for designing, analyzing, fabricating and testing IC RRs

The geometry and dimensions of the IC elements were all programmed to be driven by a single parameter, *a*, corresponding to the side of the originating cube.

Since RRs are mostly used in arrays, they are usually connected together with an illumination element. This illumination element acts as a gateway for incoming and

outgoing light and holds individual RR elements together, and it can be seen in Figure 4.4, Figure 4.5, and Figure 4.7 along with the RRs, and its thickness is represented by the parameter *t*.

4.3.1 Inverted Corner Cubes

All ICCs (*e.g.* HA and TA) can be modeled by tilting a unit cube to an angle of 54.74°, corresponding to the angle between the cube diagonal and each of its edges, about a specific vector (Zeid, 2005; Hussein *et al.*, 2016) so that the main diagonal of the cube becomes vertical, and then trimming off that rotated cube with a plane of a specific height range. The height of that trimming plane determines the aperture of the ICC element. Figure 4.3 shows the rotated/inverted cube and the height ranges for each of the HA and TA ICCs starting from the origin. Note that when cutting off the inverted cube with a plane, the lower part of the plane is the part that forms the required geometry of the ICC.

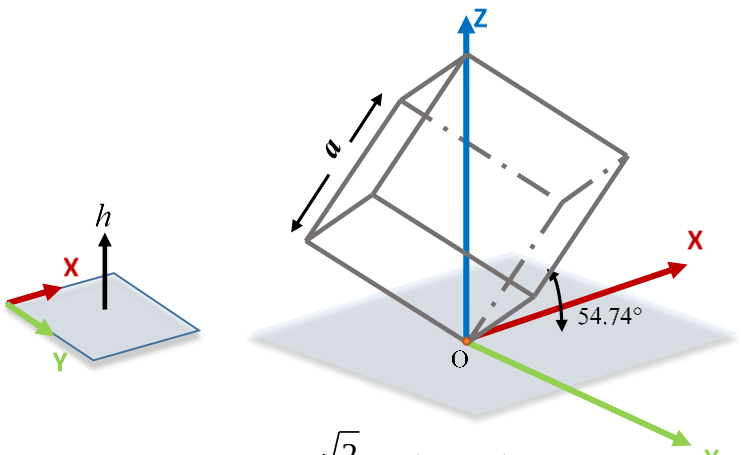

$$\text{TA ICC:} \quad 0 < h < a\frac{\sqrt{2}}{2}\sin(54.74°)$$

$$\text{HA ICC:} \quad a\left(\sqrt{3} - \frac{\sqrt{2}}{2}\sin(54.74°)\right) < h < a\sqrt{3}$$

Figure 4.3: Originating inverted cube of ICC elements

4.3.1.1 Hexagonal Retroreflective Elements

The HA ICC has a one hexagonal incident facet, and three orthogonal reflective facets. The light enters through the hexagonal facet and hits the reflective surfaces that reflect incident light using TIR and the light finally exits through the hexagonal facet in a direction parallel to that of the incident light. Figure 4.4 shows the parameters of an HA ICC which are all controlled by the side of the inverted cube a except for the parameter t corresponding to the thickness of the illumination element which is taken to be of 0.1 mm for all RR elements in this specific study.

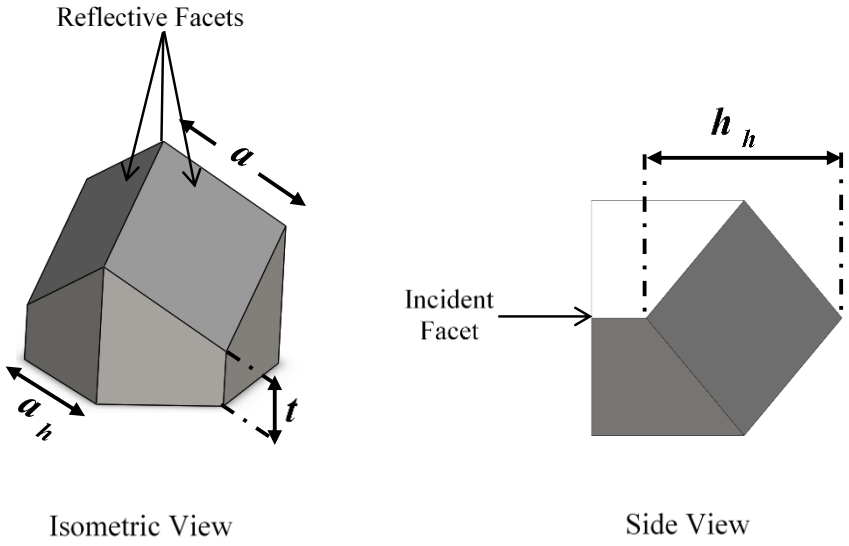

Figure 4.4: Parameters of an HA

The driving and constrained parameters of the HA IC are defined and related to each other with simple mathematical formulae in Table 4.1.

Table 4.1: Parameters of HA ICC

Hexagonal Aperture Inverted Corner Cube	
Parameter	**Equation**
Driving Parameter:	
Side of Cube [a]	a
Driven Parameters:	
Hexagon Side [a_h]	$a \times sin(54.74°)$
Height [h_h]	$a\sqrt{2} \times sin(54.74°)$
Total reflective area [$A_{r\text{-}h}$]	$3a^2$
Aperture Area [$A_{a\text{-}h}$]	$\frac{3\sqrt{3}}{2} \times a_h^2$

4.3.1.2 Triangular Retroreflective Elements

A TA ICC consists of four facets, three reflective facets and one incident facet with triangular aperture. Similarly, it can be formed from an inverted cube cut at a plane of a height of $0 < h < a\frac{\sqrt{2}}{2} sin(54.74°)$. The TA ICC geometry can also be completely constrained through the side of the inverted cube, *a*, shown in Figure 4.3 from which all other parameters can be driven (Figure 4.5). The equations deducing those parameters are presented in Table 4.2. All three reflective facets of the TA are equal isosceles triangles

and the incident facet is an equilateral triangle. Many other TA ICC geometries can be obtained by rotating the original cube to angles other than 54.74° before trimming it off with a plane. This will result with TAs with unequal areas of reflective facets which would still act as an RR. However, for this study, only the TA with equal reflective facets was considered for simplicity.

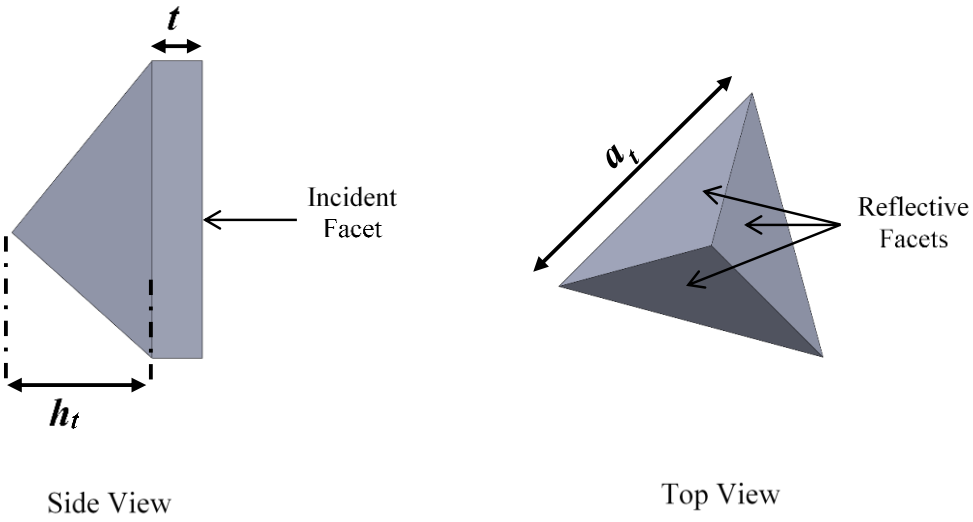

Figure 4.5: Parameters of a TA

Table 4.2: Parameters of TA ICC

Triangular Aperture Inverted Corner Cube	
Parameter	**Equation**
Driving Parameter:	
Side of Cube [a]	a
Driven Parameters:	

Side of aperture [a_t]	$a\sqrt{2}$
Height [h_t]	$\frac{a_t}{2} sin(54.74°)$
Total RR area [$A_{r\text{-}t}$]	$\frac{3}{\sqrt{4}} a_t$
Aperture Area [$A_{a\text{-}t}$]	$\frac{\sqrt{3}}{4} a_t^2$

4.3.2 Right Triangular Prisms

The parametric approached developed earlier to model the commercial HA and TA ICCs was then adapted and implemented to model the RTP elements through a set of different operations. In case of an RTP, the cube is rotated about the x-axis with an angle of -45º. This rotated cube can then be scaled up or down with a scaling function if needed. After the cube is rotated, a plane is then used to trim off the rotated cube at a certain height range as seen in Figure 4.6. The details of those operation were listed earlier in Chapter 3.

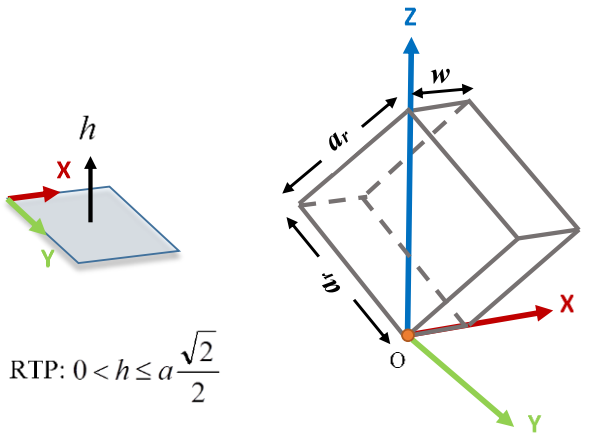

Figure 4.6: Originating unit cube of an RTP

Unlike ICCs, an RTP consists of two reflective facets and one rectangular incident facet. The parameters of a single RTP element are shown in the Figure 4.7, where all the parameters are defined with respect to side of the cube, *a*. All parameters will be defined as presented in Table 4.3.

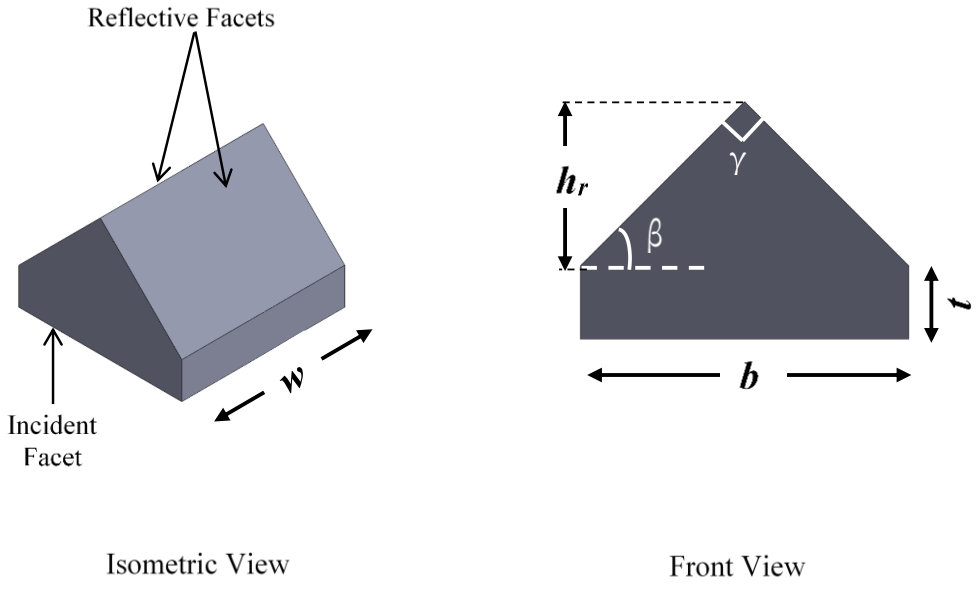

Figure 4.7: Parameters of an RTP

The base, *b*, of the RTP is dependent on the height of the cutting plane, *h*, and in this paper, *b* is calculated based on a cutting plane height of $a\frac{\sqrt{2}}{2}$. In reality, some parameters can be tailored to different conditions to optimize the performance of an RTP for different situations. For instance, the parameter β can be altered to a larger or a smaller angle to suit RTPs arranged on an inclined or curved surface rather than a flat one.

Table 4.3: Parameters of an RTP

Right Triangular Prism Inverted Cube	
Parameter	**Equation**
Driving Parameter:	
Cube side [a]	a
Driven Parameters:	
Base [b]	$a\sqrt{2}$
Width [w]	b
Beta [β]	45°
Gamma [γ]	90°
Height of RR [h_r]	$\frac{b}{2}$
Total RR area [$A_{r\text{-}r}$]	$2bw\frac{sin(\beta)}{sin(\gamma)}$
Aperture Area [$A_{a\text{-}r}$]	bw

4.4 Comparative Analysis of Retroreflective Micro-optics

The optical performances of the three IC geometries demonstrated earlier are assessed and compared to each other using an optical simulation software. A specific performance

metric was used in this study called retroreflective efficiency (RRE), which corresponds to the ratio of output light power to input light power. During the simulation tests, the RRE is measured as the light incidence angle, α, is changed from -40° to 40° to assess the RRs functionality for general safety applications.

The optical simulation set up mimics a small scale typical real life application set up, shown in Figure 4.8, in which the source first illuminates light towards the ray rotator. The ray rotator then redirects this light at the specified angle, α, to the RR elements. After entering the RR element, the light can then be retroreflected, shown in blue, reflected, shown in red, or scattered, shown in purple.

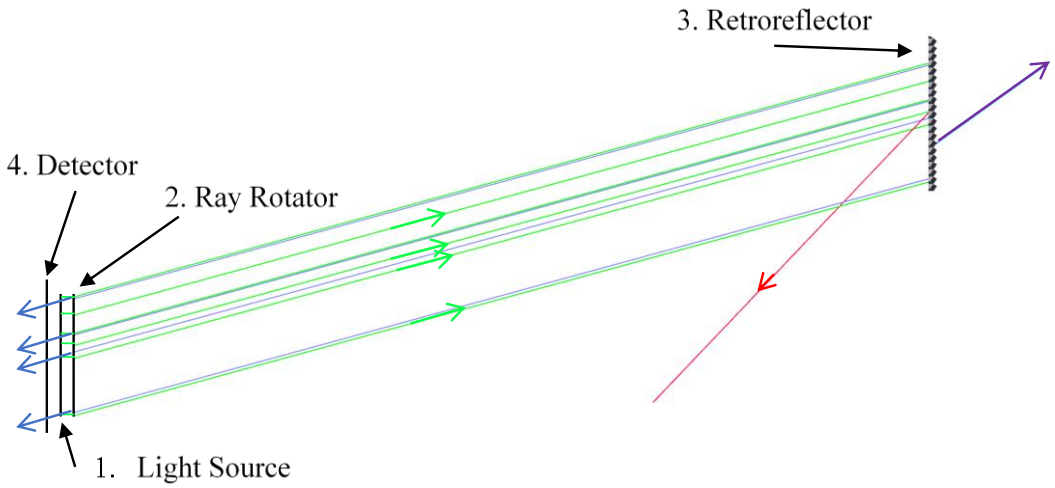

Figure 4.8: Optical simulation setup

To calculate RRE, input power is defined as all the light entering the RR element which will always be 100%, and output power is defined as the light that is exiting the RR element at an observation angle equal to the incidence angle α. Any other light that is exiting the RR element at different angles will be considered scattered or lost light (Figure 4.9). The

three elements will be evaluated at two different levels, single element level, in which one element of each geometry will be modeled and tested, and areal level, in which an array of each element will be formed and tested.

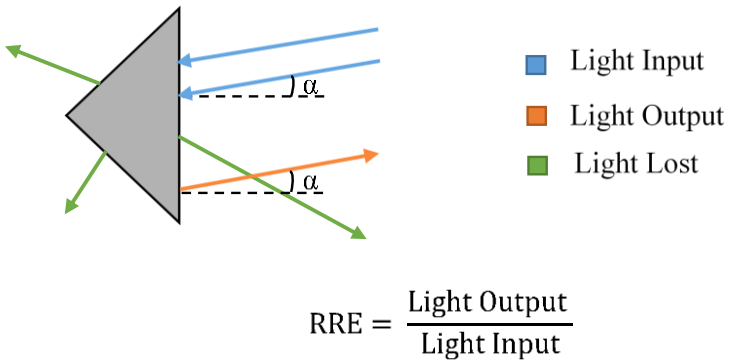

Figure 4.9: Definition of input, output and lost lights

4.4.1 Single Element Optical Performance Analysis

To compare the optical performance of the RR elements, it is important to somehow correlate their geometries. Hence, two independent analyses were done to compare the three RRs, one keeping the reflective areas of all three RRs constant, and the other by keeping their aperture areas constant. The simulations were run through Zemax OpticStudio and were validated by comparing some of the results to those obtained from previous studies (So *et al.*, 2002; Kim and Lee, 2007). Moreover, all simulations were run at constant set up distances and conditions shown in Table 4.4.

Table 4.4: Setup distances – single element analysis

Distance between source & RR	10 mm

Distance between source and detector	10.1 mm
Distance between RR and ray rotator	9.9 mm
Source power	1 W
Number of analysis rays	50000 rays

4.4.1.1 Constant Reflective Area

The reflective area of an element corresponds to the total area of all reflective facets of a single RR element. For this study, the "constant reflective area test" was done by first matching the reflective areas of the HA and TA elements to that of a 0.45 mm base RTP through CAD, which was equal to 0.2864 mm^2. The modeled geometries then were exported to the optical simulation software and their performance was analyzed and compared. Figure 4.10 shows the RRE of the RTP, HA and TA elements as the incidence angle changed from -40° to 40°.

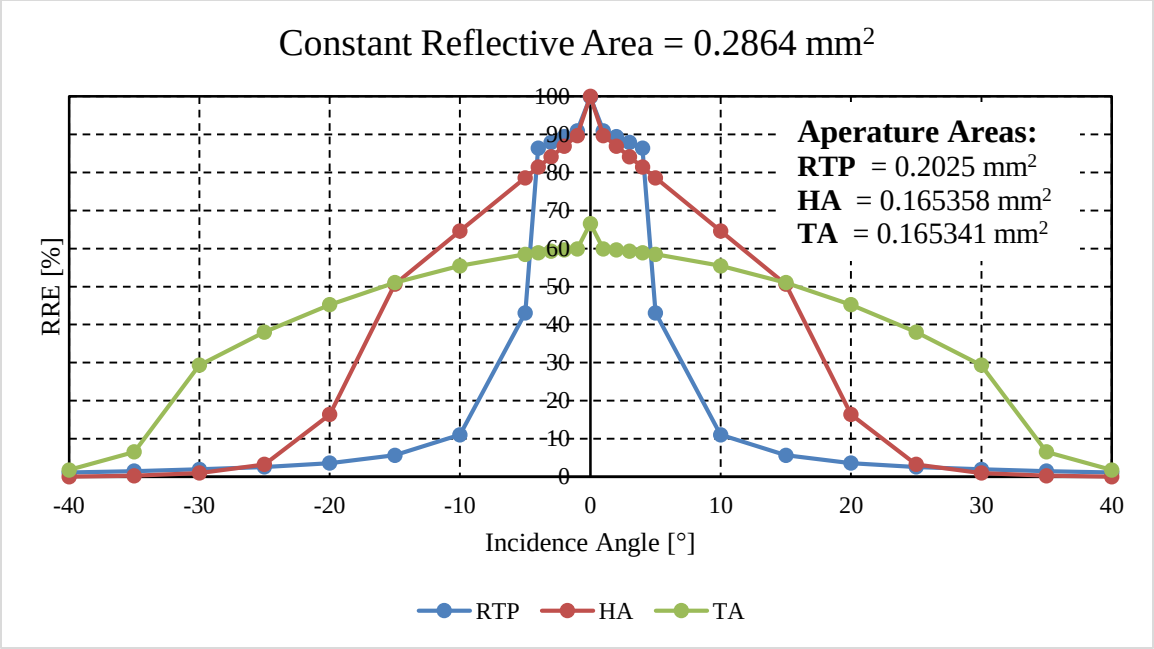

Figure 4.10: Comparision between RRE of RTP, HA, and TA with constant reflective area

When analyzing the performance of the three RRs with the same reflective area, it is noticed that RRE generally decreased as the angle of incidence increased; however, each RR showed a different declining pattern. For instance, the RTP showed the best performance at small angles (1°- 4°), but this performance rapidly deteriorated with the increase in incidence angle after 4°. The HA ICC showed a good performance up to 15° incidence angle. The TA ICC exhibited a very poor performance at smaller angles compared to other RRs, however it had the most stable pattern throughout the different incidence angles and showed superiority at incidence angles greater than 15°. Therefore, the RTP is well-suited for applications of narrow range of incidence angles, the TA ICC is advisable for applications with a wide range of incidence angle and the HA ICC can be utilized in applications requiring a small to medium incidence angles range.

Moreover, Figure 4.10 shows that at 0° incidence angle, the RRE of the TA ICC is only 66.5% compared to the 100% of the HA and RTP. This happens due to the smaller effective retroreflective area (66.5%) of the TA ICC as not the entire incident facet area contributes to retroreflection. Figure 4.11 shows the 3 corners of the incident facet that do not participate in retroreflection and are considered as dead zones and an example of a ray that is not retroreflected as it entered through one of those dead zones. This phenomenon can also be seen on the detector image in which the retroreflected light forms a hexagonal shape rather than the triangular one (Figure 4.12a). Whereas for the HA and the RTP elements, the detector displays an image that is matching to their apertures indicating a 100% effective retroreflective areas (Figure 4.12b and c).

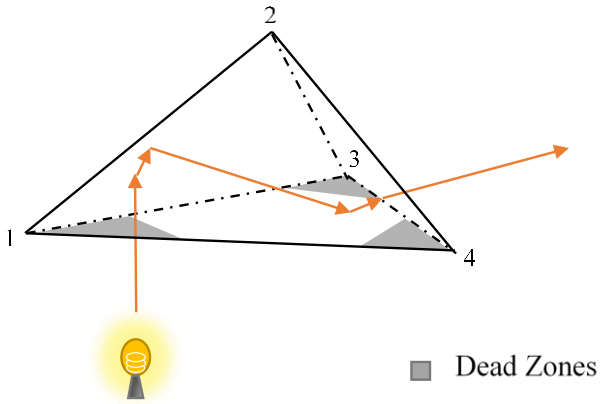

Figure 4.11: Dead zones of a TA RR

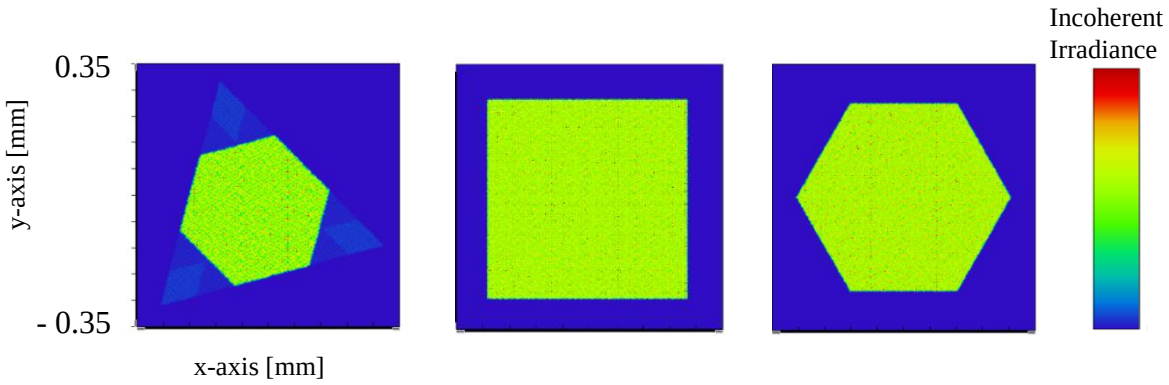

a) TA = 66.5 % **b) RTP = 100 %** **c) HA = 100 %**

Figure 4.12: Detector images of retroreflected light at 0° incidence angle

4.4.1.2 Constant Aperture Area

The next set of simulations involved changing the parameters of the HA and TA ICCs to match the aperture area of the 0.45 mm base RTP (0.2022 mm^2) to examine if having different reflective areas would yield to different results. All other conditions remained identical to the ones shown in Table 4.4. After obtaining the results, no noticeable change was seen in the RRE calculated for different incidence angles for HA and TA (Figure 4.13) to the ones presented earlier in Figure 4.10. This can be explained by the fact that all RRs were always provided with 100% input light and that the output light was always calculated relative to that.

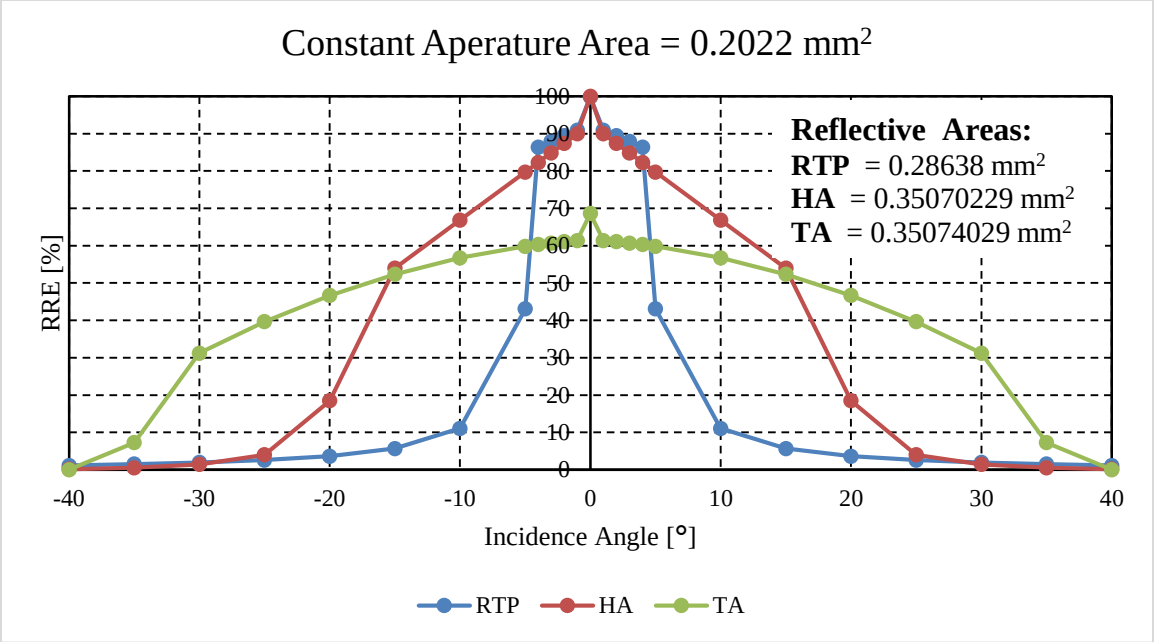

Figure 4.13: Comparision between RRE of RTP, HA, and TA with constant aperture area

Therefore, although the three geometries had different reflective areas in the second simulation set (Figure 4.13), no difference was recorded between the "constant reflective area" and the "constant aperture area" simulations.

4.4.2 Areal Optical Performance Analysis

Since RR elements are used in bundles in most applications, it is important to examine their overall optical performance as they are placed in arrays. Generally, when IC RRs are arranged in arrays, they start to cross-talk, meaning that some escaping rays of one element can enter into the neighboring element and end up being either retroreflected, reflected or lost. An example of the cross-talking phenomenon that happens between RR elements in an array is demonstrated in Figure 4.14.

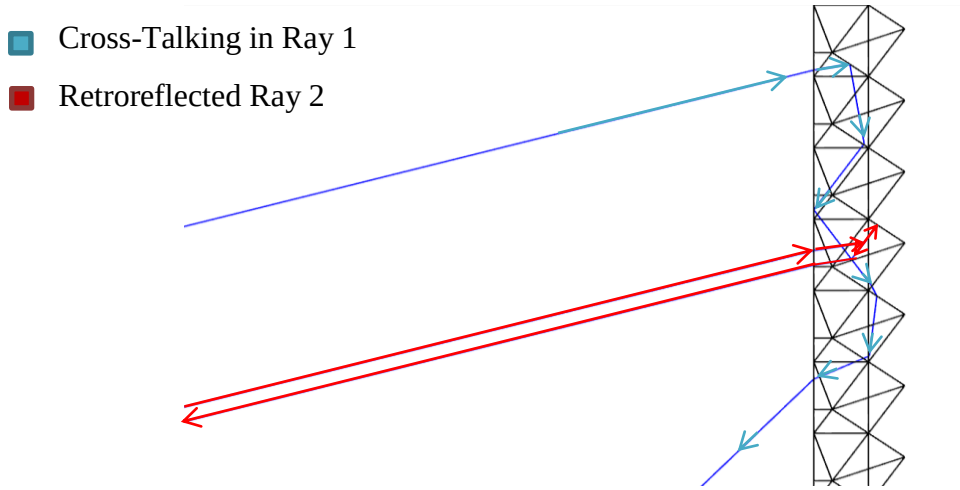

Figure 4.14: Cross talking of IC RR elements

Therefore, another set of simulations were run to test the RRE of the same RR geometries as they are aligned in arrays. Those tests were run at similar settings to the ones noted before but with different distances as shown in Table 4.5.

Table 4.5: Areal analysis test conditions

Distance between RR and source	301 mm
Distance between detector and RR	302 mm
Distance between RR and ray rotator	300 mm
Source power	1 W
Number of analysis rays	50000 rays

Three different arrays were designed on CAD, each containing 420 RR elements of the same aperture area. Figure 4.15 displays all the arrays that were used to run the simulations.

Since there was no difference between the “Constant Reflective Area” simulations “Constant Aperture Area” on the single element level, it was decided to proceed with only the “Constant Aperture Area” for the areal level analysis. Three simulations were set each running at incidence angles between -40° and 40°. All light sources were customized to match their respective RR apertures of the arrays to make sure that 100% of the light is going in.

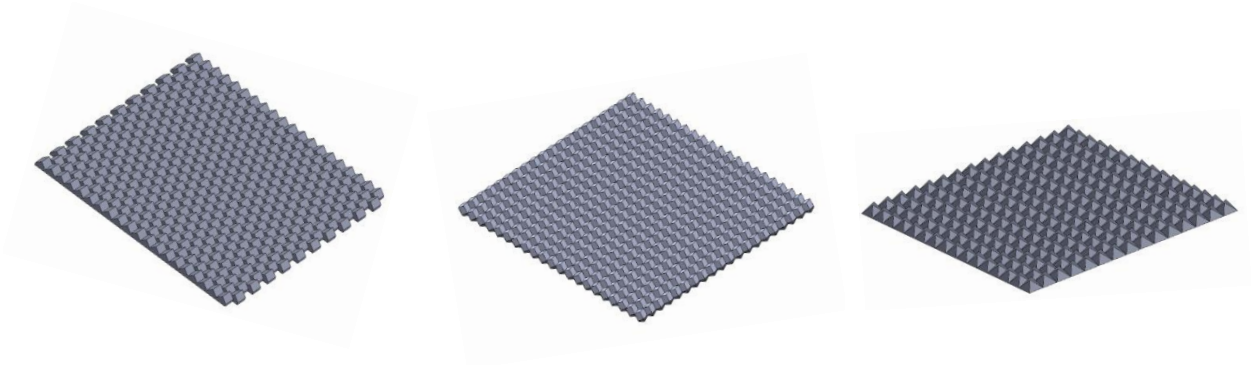

a) RTP b) HA c) TA

Figure 4.15: Arrays of a) RTP, b) HA ICC, and c) TA ICC elements

The results of the 3 simulation sets (Figure 4.16) indicate similar patterns to that of the individual elements in which the RRE generally decreases as the angle of incidence increases. Moreover, all RR arrays show results that are very close to their single elements and they all displayed almost 100% RRE at 0° incidence angle except for the TA array, which complies with the single element level results.

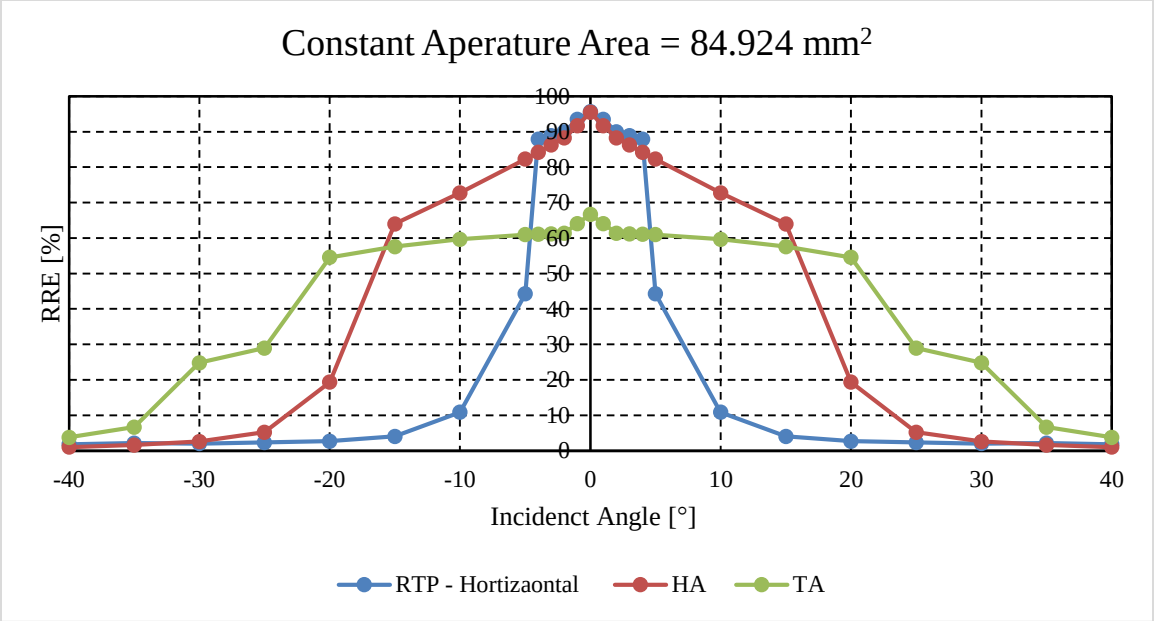

Figure 4.16: Comparative analysis between RRE of arrays of RTP, HA and TA geometries

4.5 Fabrication of IC RRs

Single IC RR elements can stand alone as functional retroreflective elements. However, if they were to be used on a broad surface area, those elements would have to be fairly thick which is not convenient for most applications. Therefore, RRs are normally used in arrays. In case of the automotive industry, the side and tail gateways are fabricated by stacking match-size hexagonal shaped pins together in the desired orientation. This stack is then placed in an electroforming bath where nickel compound is deposited on the surface of the bundled pins. That deposited piece is then used as a master mold to mass produce the plastic pieces of the vehicles' tail and side lightings which would consist of an array of ICC elements as detailed in Chapter 3. This entire method costs about $2000/in^2 to $3000/in^2 and takes 12 to 14 weeks to produce the master mold which is very expensive and time consuming.

Therefore, this study fabricates RTP arrays using a cheaper and less time consuming method called ultraprecise single point inverted cutting (USPIC) (Hamilton *et al.*, 2016a). USPIC provides two main advantages, prototyping and mass production. For instance, if a new type of RR needs to be tested, it can be directly machined by cutting through PMMA without making a master mold and if that prototype functions well, then machining can be used to cut into nickel compound to make the master mold for mass production. Moreover, USPIC is expected to reduce the time and cost of making a master mold through the conventional pin bundling methods three folds. This study uses USPIC prototyping technique to fabricate RTP arrays as they are still under the testing product development stages.

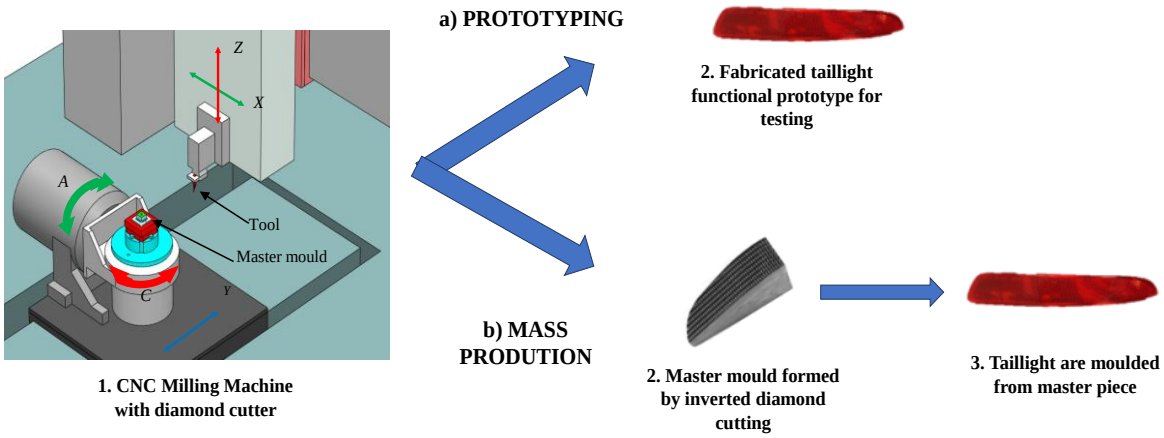

Figure 4.17: Prototyping and mass production of IC RRs through diamond cutting

4.6 Optical Performance of Fabricated Micro-Optical Elements

The fabricated RTP prototype array composed of 0.45 mm base elements was tested via luminance measuring kit and software, LMK LabSoft. The tests were carried out in a black box so that there would be no effect of outside light, and with a light source pointing

perpendicularly at the elements. Figure 4.18a presents the RTP array in the shape of the maple leaf on top of an HA RR array embedded in the taillight piece at the back, and Figure 4.18b displays the LMK luminance image showing the amount of retroreflectivity in each area. Just by looking at both Figure 4.18a and Figure 4.18b, it can be seen that most retroreflectivity is occurring at the maple leaf RTP array region. The illuminance of various regions was measured as displayed in Figure 4.18b and the results obtained show that region 1 has an average illuminance of 128.2 cd/m^2 whereas regions 2, 3, 4 and 5 displayed 50.65 cd/m^2, 39.49 cd/m^2, 96.98 cd/m^2 and 67.28 cd/m^2, respectively. These numbers indicate that the RTP array does indeed retroreflect light and in this case retains up to 135% superior RRE performance to that of the conventional HA ICC RR array. There are, however, a number of limiting factors to this test. First, the RTP prototype was fabricated through direct machining into PMMA, whereas the conventional taillight piece was manufactured through molding the PMMA using a master mold formed through pin-bundling technique, which would probably introduce radiuses at the tip of the inverted cube elements, reducing their overall RRE performance. Moreover, the difference in color between the RTP prototype and the taillight induces test inaccuracies as it is well known that the red color will absorb more light than the clear one. Hence, this test can be viewed just as a performance evaluation to prove their functionality of the RTPs rather than a comparative one. In addition, the difference in RRE performance viewed in Figure 4.18 can be used to combine different brightness areas to create artistic visual appearances for styling applications.

a) Camera Image

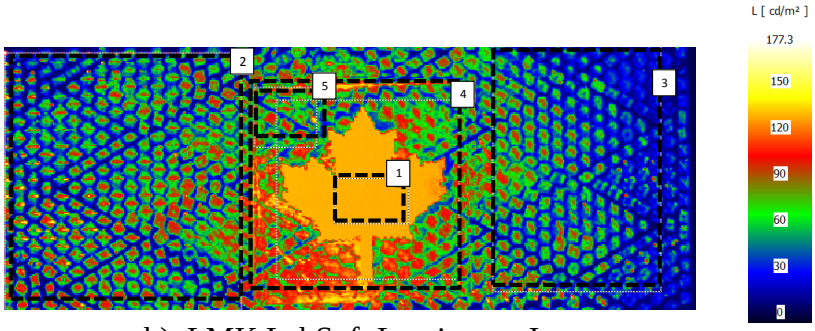

b) LMK LabSoft Luminance Image

Figure 4.18: a) Camera image and b) LMK LabSoft luminance image of RTP and HA RR arrays

4.7 Summary and Conclusions

This study presented a parametric approach of deducing inverted cube (ICC) geometries from a unit cube and implementing this approach to model RTPs and test them. A comparison analysis was completed between those structures in terms of their retroreflection efficiency (RRE) and effective retroreflective area. The analysis was conducted at both single element and areal levels of the geometries. Moreover, an array of RTPs was fabricated, tested and compared to an HA array using a luminance measuring system. The following conclusions can be drawn from the overall results:

1. RTPs function better at lower incidence angles (1°- 4°), which would make them well suited for measurement related applications, whereas HA ICCs show

superiority while at incidence angles between 10° and 15° and TA shows the most stability while operating at higher angles of incidence (more than 15°).

2. The TA IC showed an effective retroreflective area of 66.5%, while the RTP and HA ICs displayed a 100% at 0° incidence angle. Those results were directly related to the RRE of the elements and complied with results presented in previous studies (Brinksmeier *et al.*, 2008).
3. No difference was recorded between the "constant reflective area" test and the "constant aperture area" test as the output light was always noted with respect to a 100% input light power.
4. The fabricated RTP array proved to be functional as they showed comparable performance to that of the HA RR array embedded in the taillight.

4.8 Acknowledgments

This paper is the result of collaboration between Western University (London, Ontario) and Canada's National Research Council (London, Ontario). Partial financial support was also provided by Natural Sciences and Engineering Research Council (NSERC) of Canada and AUTO21 Network of Centres of Excellence. Optical simulations were facilitated with the help of CMC Microsystems through the provision of Zemax OpticStudio.

4.9 References

Brinksmeier, E., Gläbe, R. & Flucke, C. 2008. Manufacturing of molds for replication of micro cube corner retroreflectors. *Production Engineering*, **2**, 33-38.

Erickson, K. 2011. *What Neil and Buzz Left on the Moon* [Online]. NASA. Available: http://science.nasa.gov/science-news/science-at-nasa/2004/21jul_llr/ [Accessed July 26 2016].

Hamilton, B. W., Hussein, S., Milliken, N., Tutunea-Fatan, O. R. & Bordatchev, E. V. 2016a. Fabrication of Right Triangular Prism Retroreflectors Through 3½½-Axis Ultraprecise Single Point Inverted Cutting. *Computer-Aided Design and Applications*.

Hamilton, B. W., Hussein, S., Tutunea-Fatan, O. R. & Bordatchev, E. V. Fabrication of Right Triangular Prism Retroreflectors Through Ultraprecise Single Point Inverted Cutting. Manufacturing Science and Engineering Conference, April 12-15, 2016 2016b Columbia, SC, USA. ASME.

Hussein, S., Hamilton, B., Tutunea-Fatan, O. R. & Bordatchev, E. 2016. Novel Retroreflective Micro-Optical Structure for Automotive Lighting Applications. *SAE International Journal of Passenger Cars -Mechanical Systems,* **9**, 497-506.

Kim, H. & Lee, B. 2007. Optimal design of retroreflection corner-cube sheets by geometric optics analysis. *Optical Engineering,* **46**.

Liepmann, T. W. 1994. How Retroreflectors Bring the Light Back. *Laser Focus World,* **30**, 129-132.

Medicus, K. M. 2006. *Improving Measurements Based on the Cat's Eye Retro-reflection.* Doctor of Philosophy, The University of North Carolina at Charlotte.

So, B. S., Jung, Y. H. & Lee, D. W. 2002. Shape design of efficient retroreflective articles. *Journal of Materials Processing Technology,* **130**, 632-640.

Yuan, J., Chang, S., Li, S. & Zhang, Y. 2002. Design and fabrication of micro-cube-corner array retro-reflectors. *Optics Communications,* **209**, 75-83.

Zeid, I. 2005. *Mastering CAD/CAM,* McGraw-Hill Higher Education.

CHAPTER 5

General Discussion and Conclusions

5.1 Summary

This research was designed in an attempt to open the doors to modeling and exploring novel geometries of retroreflective inverted cube (IC) elements and optimizing those geometries according to the required optimum optical performance. Novel microfabrication technique developed by Hamilton et al. (Hamilton *et al.*, 2016b) was adapted to fit a newly designed retroreflective IC element called right triangular prism (RTP). This new design acquires a tool path shorter than that of the currently used IC element such as HA ICC and therefore, is expected to reduce machining time and expenses. Hence, this study concentrated on modeling and evaluation of the optical performance of those RTP structures

A parametric approach was proposed for modeling and designing RTPs to test their functionality and feasibility in general safety applications. Optical simulations were used to test the RTPs' retroreflection (RRE) at single element and areal levels as the incidence angle changed from 0° to 45°. Moreover, the effects of induced manufacturing defects or imperfections through the conventional pin bundling methods were tested through means of optical simulation and compared to those potentially fabricated through ultraprecise single point inverted cutting. Firstly, the effect of the deviation of the RTP included angle on the RRE was tested without altering any other conditions to measure the extent to which fabrication defects can be tolerated. Secondly, the optical performance of RTPs to be potentially fabricated through conventional pin bundling methods as well as inverted diamond cutting methods on a 10° inclined surface was simulated as the incidence angle changed to evaluate the effect removal of the pocket-like structures.

Furthermore, the study conducted in this thesis highlights the geometry extraction and parametrization of a number of inverted cubes (ICs), and investigates their optical performances. A comparison analysis was performed between those structures in terms of their retroreflection efficiency (RRE) and effective retroreflective area at both single element and areal levels of the geometries. In addition to the optical simulations, a functional PMMA RTP prototype array was generated through single point inverted cutting, followed by qualitative and quantitative comparative evaluations between the HA ICC element and the fabricated retroreflective RTPs were implemented using a digital lux meter as well as luminance measuring system.

5.2 Conclusions

The following can be regarded as the main contributions of this work:

1. A unified parametric approach to the geometric modeling of RR elements derived from a generic unit cube was achieved. The applicability of this approach was then demonstrated in the context of the newly proposed RTP RR geometry.

2. The functionality of areal and single element micro-RTPs was demonstrated through optical simulations and the results indicated that RRE of the analyzed RTPs decreased as the angle of incidence increased.

3. A possible major drawback of pin-bundling fabrication of RRs on inclined/freeform surfaces is associated with the presence of pocket-like features that act as light traps and thereby significantly diminish the optical performances of the retroreflective components. These manufacturing-induced imperfections can be eliminated by

means of ultraprecise single point inverted cutting that create pocket-less theoretical RTPs and hence restore their full RRE.

4. When comparing IC geometries, it was noted that RTPs functioned best at lower incidence angles (1°- 4°), which would make them well suited for measurement related applications, whereas HA ICCs showed superiority while at incidence angles between 10° and 15°, and TA showed the most stability while operating at higher angles of incidence (more than 15°).

5. The TA IC showed an effective retroreflective area of 66.5%, while the RTP and HA ICs displayed a 100% at 0° incidence angle. Those results were directly related to the RRE of the elements and complied with results presented in previous studies (Brinksmeier *et al.*, 2008).

6. The physical measurements of the retroreflected light power using the digital lux meter suggested that an RTP array prototype retains a comparable retroreflection efficiency to that of a conventional ICC RR array.

7. When tested using the luminance measuring camera and software, LMK LabSoft, the fabricated RTP array also proved to obtain a comparable illuminance to that of the HA RR array embedded in the taillight which suggests that combinations of retroreflective elements can be utilized as an approach to control visual appearance and create different artistic effects.

5.3 Strengths and Limitations

This study presented a unified parametric approach that has not been presented in earlier studies of obtaining IC geometries from unit cubes. This approach integrated a number of software such as computer-aided design (CAD) and computer-aided manufacturing (CAM) and numerical simulation programs to automate the generation of those IC geometries through a limited number of entries.

The RTPs modeled and fabricated through this parametric approach proved to be functional when compared to IC RRs through both virtual and physical test setups. Nevertheless, those RTP elements have not been tested in the context of the Society of Automotive Engineers (SAE) reflex reflectors standards (SAE, 2009) mainly due to the limitation of physical space. Moreover, the SAE standard requires tail and side lighting to be red and amber in color, whereas, the only ones tested so far were white.

Additionally, when fabricating the RTP array and comparing its performance to the HA ICC through physical tests using both the digital lux meter and the luminance measuring system, the RTP array showed superiority in terms of RRE. However, the illuminance results of both tests were inconsistent, which could be due to the different setups and test conditions.

5.4 Future Recommendations

Based on the overall results obtained in this thesis, a number of future steps are recommended to advance this work forward and to make it applicable particularly in the automotive industry and broadly in general safety applications.

For instance, aesthetics and styling is an important factor for the automotive industry as it is a means of increasing their market, therefore most automotive vehicles nowadays acquire an aerodynamic shape. Hence, it is critical to parametrically model and test RTP arrays embedded on curved surfaces to match the surface of the vehicles.

In addition, since RTPs were proved to be functional retroreflectors, they should be next adapted to fit the criteria of automotive rear and side lighting applications. Hence, optical simulations and physical tests should be done according to the procedures provided by the SAE standards for reflex reflectors (SAE, 2009).

Finally, for quality assurance, a parameter-driven optimization process of the RTP element should be done after modeling the curved RTP surfaces and performing the required tests to make sure they fit the requirements of the automotive industry. This parametric approach will also open the door to many other applications as it would be easy to optimize the RTP structures according to their needs.

5.5 References

Brinksmeier, E., Gläbe, R. & Flucke, C. 2008. Manufacturing of molds for replication of micro cube corner retroreflectors. *Production Engineering,* **2**, 33-38.

Hamilton, B. W., Hussein, S., Tutunea-Fatan, O. R. & Bordatchev, E. V. Fabrication of Right Triangular Prism Retroreflectors Through Ultraprecise Single Point Inverted Cutting. Manufacturing Science and Engineering Conference, April 12-15, 2016 2016b Columbia, SC, USA. ASME.

SAE 2009. Reflex Reflectors. *Surface Vehicle Standard.* SAE.

Appendix

Appendix A: Minimum millicandelas per incident lux for a red reflex reflector developed from SAE J594 Standard

Observation Angle (deg)	**Entrance Angle (deg) 0 deg**	**Entrance Angle (deg) 10 deg Up**	**Entrance Angle (deg) 10 deg Down**	**Entrance Angle (deg) 20 deg Left**	**Entrance Angle (deg) 20 deg Right**
0.2	420	280	280	140	140
1.5	6	5	5	3	3

Curriculum Vitae

Name: Sama Hussein

Post-secondary Education and Degrees:
University of Windsor
Windsor, Ontario, Canada
2012-2014 B.A.Sc.

The University of Western Ontario
London, Ontario, Canada
2014-2016 M.E.Sc.

Selected Honours and Awards:
Ontario Graduate Scholarship
2015-2016

Related Work Experience
Teaching Assistant
The University of Western Ontario
2014-2016

Publications:

Hussein, S., Hamilton, B., Bordatchev, E.V., and Tutunea-Fatan, O.R., 2015. Parameter-Driven Geometric Modeling of Retroreflective Features. *USB Proceedings of the* 25th *Canadian Congress of Applied Mechanics* (*CANCAM 2015*), Jun. 2015, London, Canada, pp. 96-99.

Hussein, S., Hamilton, B., Tutunea-Fatan, O., and Bordatchev, E. 2016. Novel Retroreflective Micro-Optical Structure for Automotive Lighting Applications. *SAE Int. J. Passeng. Cars - Mech. Syst*. **9**(2):497-506, doi:10.4271/2016-01-1407.

Hussein, S., Hamilton, B., Bordatchev, E.V., and Tutunea-Fatan, O.R. 2016. Optical Performance of Right Triangular Prism *Proceedings of the Photonics North 2016 Conference*. May 2016, Quebec City, Canada.

Hamilton, B., Milliken, N., Hussein, S., Tutunea-Fatan, O. R. & Bordatchev, E. V. 2016. Fabrication of Right Triangular Prism Retroreflectors through 3 1/2 1/2-Axis Ultraprecise Single Point Inverted Cutting. Computer-Aided Design and Applications.

Hamilton, B., Hussein, S., Tutunea-Fatan, O. R. & Bordatchev, E. V. 2016. Fabrication of Right Triangular Prism Retroreflectors through Ultraprecise Single Point Inverted Cutting. Manufacturing Science and Engineering Conference. Blacksburg, Virginia.

Hamilton, B., Hussein, S., Tutunea-Fatan, O.R., and Bordatchev, E.V., 2015, "Strategies in Single Point Inverted Cutting for Fabrication of Structured Surfaces," USB Proceedings of the *25th Canadian Congress of Applied Mechanics (CANCAM 2015)*, Jun. 2015, London, Canada, pp. 108-111.

Hamilton, B., Milliken, N., Hussein, S., Tutunea-Fatan, O. R. & Bordatchev, E. V. 2016. Enhanced Bidirectional Fabrication of Right Triangular Retroreflectors. *American Society of Precision Engineering 31st Annual Meeting*. Submitted.